The Astrophysical Journal, 770:114 (18pp), 2013 June 20 doi:10.1088/0004-637X/770/2/114

STELLAR POPULATIONS IN COMPACT GALAXY GROUPS: A MULTI-WAVELENGTH STUDY OF HCGs 16, 22, AND 42, THEIR STAR CLUSTERS, AND DWARF GALAXIES

I. S. Konstantopoulos[1,14], A. Maybhate[2], J. C. Charlton[3], K. Fedotov[4,5], P. R. Durrell[6], J. S. Mulchaey[7], J. English[8], T. D. Desjardins[4], S. C. Gallagher[4], L. M. Walker[9], K. E. Johnson[9,10], P. Tzanavaris[11,12], and C. Gronwall[3,13]

[1] Australian Astronomical Observatory, P.O. Box 915, North Ryde, NSW 1670, Australia; iraklis@aao.gov.au
[2] Space Telescope Science Institute, 3700 San Martin Drive, Baltimore, MD 21218, USA
[3] Department of Astronomy and Astrophysics, The Pennsylvania State University, 525 Davey Lab, University Park, PA 16802, USA
[4] Department of Physics and Astronomy, The University of Western Ontario, London, ON N6A 3K7, Canada
[5] Herzberg Institute of Astrophysics, Victoria, BC V9E 2E7, Canada
[6] Department of Physics and Astronomy, Youngstown State University, Youngstown, OH 44555, USA
[7] Carnegie Observatories, Pasadena, CA 91101, USA
[8] Department of Physics and Astronomy, University of Manitoba, Winnipeg, Manitoba R3T 2N2, Canada
[9] Department of Astronomy, University of Virginia, P.O. Box 3813, Charlottesville, VA 22904, USA
[10] National Radio Astronomy Observatory, 520 Edgemont Road, Charlottesville, VA 22903, USA
[11] Laboratory for X-ray Astrophysics, NASA Goddard Space Flight Center, Greenbelt, MD 20771, USA
[12] Department of Physics and Astronomy, The Johns Hopkins University, Baltimore, MD 21218, USA
[13] Institute for Gravitation and the Cosmos, The Pennsylvania State University, University Park, PA 16802, USA

Received 2013 March 10; accepted 2013 April 17; published 2013 June 3

ABSTRACT

We present a multi-wavelength analysis of three compact galaxy groups, Hickson compact groups (HCGs) 16, 22, and 42, which describe a sequence in terms of gas richness, from space- (*Swift*, *Hubble Space Telescope* (*HST*), and *Spitzer*) and ground-based (Las Campanas Observatory and Cerro Tololo Inter-American Observatory) imaging and spectroscopy. We study various signs of past interactions including a faint, dusty tidal feature about HCG 16A, which we tentatively age-date at <1 Gyr. This represents the possible detection of a tidal feature at the end of its phase of optical observability. Our *HST* images also resolve what were thought to be double nuclei in HCG 16C and D into multiple, distinct sources, likely to be star clusters. Beyond our phenomenological treatment, we focus primarily on contrasting the stellar populations across these three groups. The star clusters show a remarkable intermediate-age population in HCG 22, and identify the time at which star formation was quenched in HCG 42. We also search for dwarf galaxies at accordant redshifts. The inclusion of 33 members and 27 "associates" (possible members) radically changes group dynamical masses, which in turn may affect previous evolutionary classifications. The extended membership paints a picture of relative isolation in HCGs 16 and 22, but shows HCG 42 to be part of a larger structure, following a dichotomy expected from recent studies. We conclude that (1) star cluster populations provide an excellent metric of evolutionary state, as they can age-date the past epochs of star formation; and (2) the extended dwarf galaxy population must be considered in assessing the dynamical state of a compact group.

Key words: galaxies: dwarf – galaxies: evolution – galaxies: groups: individual (HCG 16, HCG 22, HCG 42) – galaxies: interactions – galaxies: star clusters: general – intergalactic medium

Online-only material: color figures

1. INTRODUCTION

The classical formulation of a compact group (CG) of galaxies defines an assortment of typically three or four densely packed large galaxies (Hickson 1982; Barton et al. 1996). As such, CGs represent the upper end of the surface/volume density distribution in the local universe. The recent advent of large spectroscopic studies and simulations of large-scale structure have enabled researchers to quantify the surroundings of CGs, and discover an even division between truly isolated systems and those embedded in larger groupings (most notably McConnachie et al. 2009; Mendel et al. 2011). Their importance in the context of galaxy evolution therefore becomes evident when considering the possible end states that can arise from such assortments of galaxies. Isolated groups may give rise to field ellipticals, while embedded groups might be the sites of galaxy pre-processing, where spiral galaxies deplete their gas supply and morph into lenticulars before falling into the nearest deep potential well, and eventually become the ingredients of a dry merger.

A number of works have quantified the evolutionary state of CGs, starting from the cool gas content—a proxy of the available reservoir for star formation. Verdes-Montenegro et al. (2001) established that CGs are deficient in H I gas when compared to field galaxies of like morphology, while Johnson et al. (2007) compared the ratio of gas-to-total mass to establish a rudimentary evolutionary sequence. In Konstantopoulos et al. (2010), we expanded on this concept by dividing groups into dual, parallel sequences, with one track for groups where gas is contained within the member galaxies (Type A), and another for those groups that feature an intragroup medium (IGM), be it in cold, warm, or hot gas (Type B). The end points of the two sequences differ significantly, in that only the enhanced-IGM sequence should develop an X-ray halo, such as those seen around massive elliptical galaxies. This is an important feature, as the typically shallow CG potential well cannot build up a hot gas halo, with, perhaps, the exception of the most massive CGs.

[14] I.S.K. is the recipient of a John Stocker Postdoctoral Fellowship from the Science and Industry Research Fund.

This was supported by Desjardins et al. (2013), who recently found the X-ray emission in several Hickson compact groups (HCGs) to be concentrated mostly around individual galaxies. Collisions between galaxies and the IGM, however, can produce an X-ray halo, an effect common among groups with high velocity dispersions (e.g., in Stephan's Quintet; Bahcall et al. 1984; Sulentic et al. 1995).

One aspect of CGs that has been limited in the past is dwarf galaxy membership. Since dense environments are likely to process dwarfs more efficiently through accretion and infall (Mobasher et al. 2003), the study of dwarfs is potentially a topic of particular importance to CG evolution. Only a few studies have touched upon this, such as the statistical work by Hunsberger et al. (1998; part of a study of the CG luminosity function) and the study of ultracompact dwarf (UCD) formation by Da Rocha et al. (2011). Zabludoff & Mulchaey (1998, 2000) examined the dwarf populations of several loose groups, and included HCG 42 in their study. The dwarf galaxy population of HCG 42 was further enhanced by samples observed by de Carvalho & Coziol (1999) and Carrasco et al. (2006), bringing the membership to a few dozen potential dwarf members. In our previous works on HCGs 7 and 59 we included spectroscopic samples complete to $R \approx 18$, but that only covers a few dwarf galaxies in each group, e.g., the single detection in HCG 7. Our incomplete understanding of the CG luminosity function (and therefore dwarf membership) has potentially adverse effects on various measurements. While we routinely use metrics well suited to galaxy clusters, such as the velocity dispersion, their true value when derived from three or four elements is highly uncertain (as concluded by McConnachie et al. 2008).

At the same time, the stellar populations of CGs have been the focus of numerous studies. Since star formation and galaxy evolution go hand-in-hand, much that is known about the latter has come about by studying the colors of CG galaxies (e.g., infrared colors; Gallagher et al. 2008; Bitsakis et al. 2011; Walker et al. 2012; Cluver et al. 2013) and the properties of their star clusters—be it old globular clusters (GCs; Da Rocha et al. 2002), or massive star clusters of young and intermediate age (Palma et al. 2002; Gallagher et al. 2010; Fedotov et al. 2011; Konstantopoulos et al. 2010, 2011, 2012). The GCs show mostly regular characteristics, with some groups hosting poor populations (NGC 6868; Da Rocha et al. 2002), and young star clusters have been successfully used as chronometers of past dynamical events in HCG 92 (Stephan's Quintet; Fedotov et al. 2011). While the potential is great, it comes at a great cost, as the *Hubble Space Telescope* (*HST*) offers the only currently suitable instrumentation for definitively distinguishing star clusters in wide extragalactic fields from foreground stars and background galaxies (e.g., Schweizer 2004; Konstantopoulos et al. 2013). Given the propensity of CGs for interactions, intragroup stellar populations should also be common. The study by Da Rocha & Mendes de Oliveira (2005) found the intragroup light of HCG 79 to be consistent with an old population, indicative of either ancient interactions or old stars stripped in a recent event. One evolutionary step ahead of intragroup light, in HCG 59 we found a tidal bridge connecting two galaxies, and roughly dated its emergence to within the past Gyr (Konstantopoulos et al. 2012; White et al. 2003).

In recent work, we have pursued an understanding of galaxy evolution in CGs through multi-wavelength studies of individual groups (Gallagher et al. 2010; Konstantopoulos et al. 2010, 2012) and larger samples alike (Hunsberger et al. 1998; Johnson et al. 2007; Gallagher et al. 2008; Tzanavaris et al. 2010; Walker et al. 2010, 2012; Desjardins et al. 2013). This work continues the series by contrasting the stellar populations of three CGs, HCG 16, 22, and 42, in search of evolutionary trends. We choose these groups as they encompass the full sequence of gas richness defined in Johnson et al. (2007) and Konstantopoulos et al. (2010): HCG 16 is Type IB, HCG 22 is Type IIA, and HCG 42 is Type IIIA (the notation of this classification system is outlined in Section 2). We examine the colors of young and old star clusters, which proxy their ages, to trace ongoing star formation, the recent star formation history, and past merger events. Specifically, we seek a reflection of the evolving evolutionary state of the HCG 16–22–42 sequence in the star cluster age distribution (see the starburst and interaction dating of Konstantopoulos et al. 2009; Fedotov et al. 2011). In order to establish the star formation history diagnostic most appropriate to CGs, we compare star cluster colors to broadband metrics in the UV, optical, and IR, and stacked wide-field images where we search for tidal features. Finally, we examine the dwarf galaxy populations by collating past surveys and combining with new and previously unpublished spectroscopy. We look for an assessment of the importance of including the dwarfs in characterizations of the stellar populations, and the derivation of dynamical masses.

2. OVERVIEW OF HCGs 16, 22, AND 42 AND RELATED LITERATURE

Table 1 gives an overview of the positional, physical, morphological, photometric, and nuclear properties of 11 galaxies in the 3 CGs we study in this paper. The early-type galaxy content increases along the 16–22–42 sequence and the neutral gas content decreases, but other characteristics are not as neatly defined. HCG 16 hosts at least two active galactic nuclei (AGNs; Turner et al. 2001) and a starburst, while star formation and nuclear activity is lower in the two other groups. Regarding the J07/K10 evolutionary type (Johnson et al. 2007; Konstantopoulos et al. 2010), the roman numerals describe decreasing gas richness (Type I is rich), while the latter discriminates between Sequence A of groups with gas contained in individual galaxies, and Sequence B, containing groups that show evidence of an IGM. We note that the A/B type of HCG 42 cannot be confidently constrained, as it is uncertain whether the diffuse X-ray emission is connected to the IGM, or galaxy 42A alone (Desjardins et al. 2013). We refer to this group as Type IIIA throughout this paper.

HCG 16 has been studied from several points of view. de Carvalho et al. (1997) updated its dwarf galaxy population by including three new members, thus increasing the velocity dispersion of the group by $\approx$65 km s^{-1} to 400 km s^{-1}. The merger history of this CG was investigated by de Carvalho & Coziol (1999), who suggest that both group lenticulars, 16C and 16D, are remnants of recent mergers, as traced by double spectroscopic nuclear peaks. HCG 16 is described by Belsole et al. (2003) as a collapsed group at the low-luminosity end of X-ray emitters, while Rich et al. (2010) trace a biconical polar outflow in 16D with optical integral-field spectroscopy, which resembles the superwind in M82 (recently revisited by Desjardins et al. 2013). They also detect an intermediate-age ($\sim$400 Myr) A-star population that is rapidly rotating, consistent with the large sample of lenticular galaxies studied by Emsellem et al. (2011). In a very recent work, Vogt et al. (2013) revisited the galactic winds of HCG 16. The HCG 16D wind was characterized as symmetric and shock-excited, while the outflow in 16C was found to be asymmetric due to the interaction with

Table 1
HCGs 16, 22, and 42: Positional, Morphological, Photometric, and Nuclear Properties, and Measured Masses

Identifier	Coordinates (J2000)	Type	m_R (mag)	v_R (km s^{-1})	$M*$ ($\times 10^9$ $M_\odot$)	$M_{\rm H\,I}$	SFR ($M_\odot$yr^{-1})	sSFR ($\times 10^{-10}$yr^{-1})	Nucleus	References
HCG 16										
A: NGC 0835	02 09 24.6 −10 08 09	SBab	12.30	4073	2.65	1.17	5.37 ± 0.62*	3.68 ± 0.57	AGN	1, 1, 7, 13
B: NGC 0833	02 09 20.8 −10 07 59	Sab	12.65	3864	1.03	0.79	0.33 ± 0.03*	0.43 ± 0.07	AGN	1, 1, 7, 13
C: NGC 0838	02 09 38.5 −10 08 48	Im	12.82	3851	1.19	3.02	14.38 ± 1.83	21.19 ± 4.10	SB	2, 1, 1, 13
D: NGC 0839	02 09 42.9 −10 11 03	Im	13.86	3874	1.03	>4.47	17.06 ± 2.31	30.10 ± 5.80	AGN	3, 5, 6, 13
HCG 22										
A: NGC 1199	03 03 38.4 −15 36 48	E2	10.95	2570	2.09	···	0.24 ± 0.02	0.21 ± 0.03	A	2, 6, 9, 14
B: NGC 1190	03 03 26.1 −15 39 43	Sa	13.64	2618	0.14	···	0.03 ± 0.01	0.38 ± 0.07	A	4, 6, 3, 14
C: NGC 1189	03 03 24.5 −15 37 24	SBcd	13.19	2544	0.15	<1.35	0.46 ± 0.04	5.64 ± 0.95	E	3, 6, 10, 14
HCG 42										
A: NGC 3091	10 00 14.3 −19 38 13	E3	10.31	3964	4.73	4.35	0.44 ± 0.04*	0.17 ± 0.03	AGN	3, 6, 9, 14
B: NGC 3096	10 00 33.1 −19 39 43	SB0	13.03	4228	0.80	···	0.10 ± 0.03	0.23 ± 0.07	A	4, 6, 3, 14
C: MCG -03-26-006	10 00 10.3 −19 37 19	E2	12.86	4005	0.86	···	0.09 ± 0.02	0.18 ± 0.04	A	4, 6, 11, 14
D: PGC 028926	10 00 13.0 −19 40 23	E2	14.73	4042	0.13	···	0.01 ± 0.01	0.15 ± 0.07	A	3, 6, 12, 14

Notes. Morphological types from Hickson et al. (1989). Stellar masses, star formation rates (SFR), and specific SFRs (sSFR) are drawn from Tzanavaris et al. (2010), corrected for a known M_* overestimation factor of 7.4 (P. Tzanavaris 2012, private communication). $M_{\rm H\,I}$ values from Verdes-Montenegro et al. (2001; individual galaxies in HCG 16), Price et al. (2000; HCG 22), and Huchtmeier (1994) for the entirety of HCG 42, contained within the quoted HCG 42A beam. Nuclear classifications of "A" and "E" stand for absorption- and emission-line-dominated spectra. References are given in sequences representing positions, magnitudes, radial velocities, and nuclear classification: (1) York et al. 2000; (2) Evans et al. 2010; (3) de Carvalho et al. 1997; (4) Skrutskie et al. 2006; (5) Doyle et al. 2005; (6) Hickson et al. 1989; (7) Ribeiro et al. 1996; (8) Paturel et al. 2003; (9) Huchtmeier 1994; (10) Monnier Ragaigne et al. 2003; (11) Hickson et al. 1992; (12) Carrasco et al. 2006; (13) Turner et al. 2001; (14) P. Tzanavaris et al., in preparation. Asterisks (*) denote SFR values that are potentially contaminated by AGNs.

the H I envelope into which the wind is advancing, and the excitation mechanism was attributed to a blend of photoinization and slow shocks.

The GC population of HCG 22A was studied with ground-based optical imaging by Da Rocha et al. (2002), who estimate a specific frequency (number of clusters per unit brightness) of $S_N = 3.6 \pm 1.8$, consistent with its morphological type of E3. The GCs trace a bimodal color distribution with peaks at $(B - R)_0 = 1.13, 1.42$ mag, a common occurrence in early-type galaxies (e.g., Brodie & Strader 2006). Da Rocha et al. (2011) discovered a population of 16 UCD galaxies in HCG 22, and used them to suggest two channels of UCD formation: old, metal-poor star clusters, and stripped dwarf galaxies with higher metallicities and mixed (or young) stellar populations.

As described above, HCG 42 was one of the poor groups studied by Zabludoff & Mulchaey (1998, 2000) as part of a dwarf galaxy survey. Combined with de Carvalho et al. (1997) and Carrasco et al. (2006), these works have identified dozens of galaxies related to the group. We will be following up on this aspect with particular interest over the following sections.

3. OBSERVATIONS

The work presented in this paper is based on new and archival data from ground- and space-based observatories, which we summarize in Table 2. We use optical imaging from the Las Campanas Observatory (LCO) DuPont telescope (Direct CCD Camera and Wide Field Imaging CCD Camera) in the *B* and *R* bands, taken at the same time as the images presented in Konstantopoulos et al. (2010). We therefore refer the reader to that paper for details on the observational setup, as well as the data acquisition and reduction. In the case of HCG 16, the LCO images are complemented by Sloan Digital Sky Survey (SDSS; York et al. 2000) imaging in the *ugriz* filter set.

Multi-wavelength imaging comes from the *Chandra*, *Swift*, *HST*, and *Spitzer* space telescopes. Archival data are drawn from the Chandra X-ray Center and the NASA/IPAC Infrared Science Archive for post-basic calibration *Spitzer* imaging in the four IRAC bands. We make use of the same *Swift* UV/Optical Telescope (UVOT) data set presented in Tzanavaris et al. (2010; we refer the reader there for details), which includes images in the *w2*, *m2*, and *w1* filters (central wavelengths of 1928, 2246, and 2600 Å; Poole et al. 2008). *HST* images from the WFPC2 and ACS/WFC cameras were reduced on-the-fly using the *Mikulski Archive for Space Telescopes*. WFPC2 data were then processed with `MultiDrizzle` to register each chip separately, before correcting the photometry for charge transfer inefficiencies using the prescription of Dolphin (2000). *HST* coverage consisted of multiple pointings, as listed in Table 2. Star formation in HCG 22 was studied through Fabry-Perot data by Torres-Flores et al. (2009), who found a number of blue regions of the intra-group medium, indicating galaxy-galaxy interactions in the not-so-distant past.

We also make use of new spectroscopy from Cerro Tololo Inter-American Observatory (CTIO)-Hydra and previously unpublished spectra from the DuPont telescope (Multifiber Spectrograph and 2D-FRUTTI). The Hydra observations were taken with a combination of the KPGL2 grating ($R \sim 4400$) and GG385 blocking filter, tuned to a central wavelength of 5800 Å, and are described in Konstantopoulos et al. (2010). The Magellan spectra were taken on the same observing run as the data used for Zabludoff & Mulchaey (1998), so we refer readers there for details of the acquisition and reduction. In brief, the wavelength coverage extends between 3500 and 6500 Å, at a resolution of ∼5–6 Å (3 Å pixel^{-1} dispersion).

3.1. Star Cluster Selection

The star cluster analysis that will follow in Section 5.1 is based, for the most part, on WFPC2 images. The exception is the cluster population of HCG 42A, which makes use of Advanced Camera for Surveys (ACS) data. In this case, we follow

Table 2
Summary of Imaging Observations

Target	Instrument	Filter	Date	t_{exp} (s)	Program ID
HST					
HCG 16	WFPC2	F435W	2007 Jul 17	1900	10787
...	...	F606W	2007 Jul 17	1900	...
...	...	F814W	2007 Jul 23	1900	...
HCG 22	...	F435W	2007 Sep 21	1900	...
...	...	F606W	2007 Sep 21	1900	...
...	...	F814W	2007 Sep 21	1900	...
HCG 42	...	F435W	2007 Nov 13	4200	...
...	...	F606W	2007 Nov 13	4200	...
...	...	F814W	2007 Nov 13	4200	...
...	ACS-WFC	F435W	2007 Dec 4	1710	...
...	...	F606W	2007 Dec 6	1230	...
...	...	F814W	2007 Dec 8	1080	...
Swift					
HCG 16	UVOT	UVW2	2007 Feb 24	4652	–[a]
...	...	UVM2	2007 Feb 24	3894	–
...	...	UVW1	2007 Feb 24	2596	–
HCG 22	...	UVW2	2007 Mar 17	3650	–
...	...	UVM2	2007 Mar 17	3214	–
...	...	UVW1	2007 Mar 17	2524	–
HCG 42	...	UVW2	2007 Feb 1	3326	–
...	...	UVM2	2007 Feb 1	3027	–
...	...	UVW1	2007 Feb 1	2017	–
LCO-100″					
HCG 16	CCD	JB	2007 Oct 5	180	–
...	...	KC-R	2007 Oct 3	120	–
HCG 22	...	JB	2007 Oct 6	120	–
...	...	KC-R	2007 Oct 4	120	–
HCG 42	WFCCD	B	2008 May 8	110	–
...	...	R	2008 May 6	600	–
Spitzer					
HCG 16	IRAC	3.6–8.0 μm	2005 Jan 17	27	3596
HCG 22	...	3.6–8.0 μm	2005 Jan 17	27	...
HCG 42	...	3.6–8.0 μm	2004 Dec 17	27	...

Note. [a] The *Swift* observations were taken as a Team Project, and are not associated with a program ID.

the methodology presented in Konstantopoulos et al. (2010, 2012) to select clusters. In brief, we selected star clusters with `IRAF-DAOfind`[15] and filter according to a metric of central concentration that is based on point-spread function photometry (employing a custom-made function), before applying a brightness cut at $M_V < -9$ mag.

In the case of WFPC2, the lower resolution does not allow for such filtering. Instead, we performed a more thorough selection process rather than filtering a long list. First, we divided each image by the square root of its median to create a frame with uniform noise. Such a detection image was created for each individual chip, each pointing, and each filter. We then performed an `IRAF-DAOfind` search and cross-correlated the resulting detection lists, promoting only sources that appeared in two or more lists to the final source catalog. Photometry was then performed in each original image. Unfortunately, it was not possible to further filter through WFPC2 source photometry, so we did so a through visual inspection of all sources with $M_V < -9$ mag. This eliminated the vast majority of background galaxies, as their surface brightness profiles differ largely from those of star clusters. While it is not trivial to quantify the expected degree of contamination by background galaxies, we note that spirals are expected to span the entire sequence of star clusters colors (from a few Myr to GC colors), depending on their star formation rate (SFR) and history, and dust content. This would preclude regions in color space from being devoid of data points. As will be shown in Section 5, we do observe such voids, which suggests the degree of contamination from background galaxies is low. Not all stars were removed, however, as those are largely indistinguishable from clusters at the distances studied and with the WFPC2 image scale. We therefore expect some stellar contamination at the red end of star cluster color space.

The 50% and 90% completeness fractions for our WFPC2 star cluster selection were estimated by generating artificial sources with `MKSynth` (part of the `BAOLAB` suite; Larsen 1999) and testing their recovery through the detection method described above. We generated a 10×10 grid of artificial sources and inserted them into the images of two galaxies per group, in order to cover varying morphologies. The grid covered both galaxy and background, as we wish to assess the observability of star clusters throughout these CGs. Our estimates therefore present a best-case scenario for spiral and irregular systems, where crowding and variable extinction will further complicate detection. However, the detection limits should be taken at face value in the case of early-type galaxies, as their smooth profiles do not inhibit detection. Figure 1 plots the curves, from which we derive [90%, 50%] completeness fractions of roughly [25, 26] mag in HCGs 16, 22, and [25.5, 26.5] mag in HCG 42. These are all fainter than the brightness cut applied at $M_V = -9$ mag, therefore we treat our star cluster catalogs as luminosity-limited. It is important in studies of star cluster populations to understand the detection limit not only in terms of brightness, but also mass. Since the mass-to-light ratio of a simple stellar population (SSP) evolves with time, the mass required for a star cluster to be detected will change with its age. Figure 2 investigates this relation by translating the limiting brightness of a Marigo et al. (2008) model SSP into the corresponding mass. We estimate completeness over the past [1, 10] Gyr to masses of $[1, 5] \times 10^5\ M_\odot$.

4. PHENOMENOLOGY

Figures 3–5 show *HST* imaging (*BVI*) and color composites of *Swift* (UV, blue), LCO (*R* band, green), and *Spitzer* (3.6 μm, red) frames, which we use to study the large-scale properties of the groups and individual galaxies. Blue emission indicates star formation over the past ≈100 Myr, while older populations shine in red and yellow (photospheres shine in *V*-band continuum and 3.6 μm). Hα emission is covered in the *R* band, so ongoing star formation will appear purple or pink. Visual inspection shows all galaxies to be consistent with their published morphological types. We note a lopsided appearance in HCG 16B, highlighted by the isophotes of the high-contrast image of Figure 7. The "patchy" dust distribution of HCG 16C is seen both as reddening in the optical, and a red/white appearance in the multi-wavelength imaging. We also note the strong bar of HCG 22C and the low surface brightness of its spiral arms, the only part of the image that registers significant UV flux. Finally, we note a "boxy" bulge-disk appearance in HCG 42B, both in the optical image, and in stellar photospheric emission (*R* band, 3.6 μm). The following sections will visit small-scale features in HCGs 16, 22, and 42.

[15] IRAF is distributed by the National Optical Astronomy Observatories, which are operated by the Association of Universities for Research in Astronomy Inc., under cooperative agreement with the National Science Foundation.

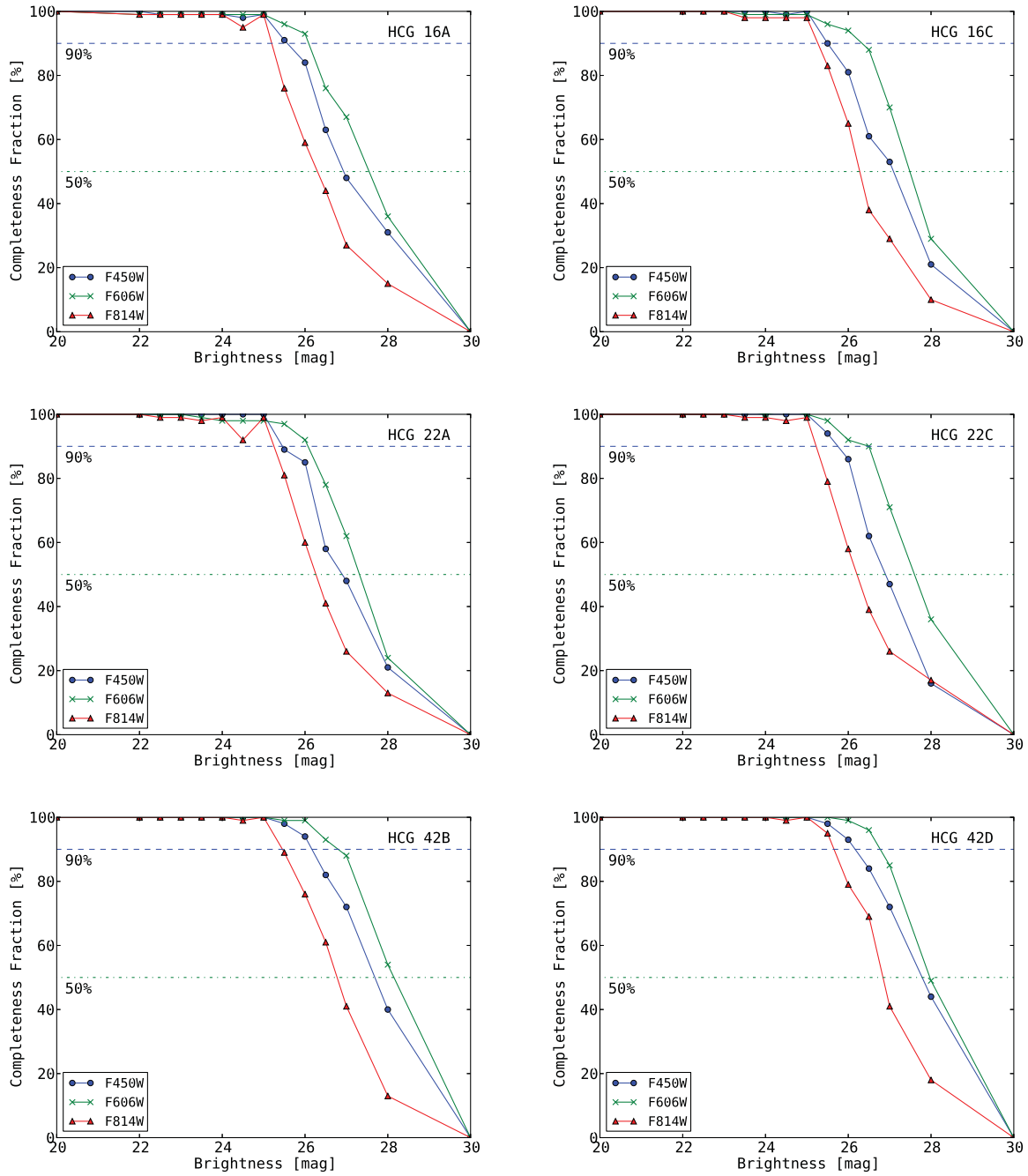

Figure 1. Completeness tests for star cluster detections in HCGs 16, 22, and 42. We test two galaxies per group to cover different environments, namely, early- vs. late-type galaxies. I_{814} is always the limiting filter, and defines the 90% and 50% completeness fractions as roughly 25, 26 mag in HCGs 16, 22, and 25.5, 26.5 mag in HCG 42.

(A color version of this figure is available in the online journal.)

4.1. Central Sources in HCG 16C and D

Taking advantage of the high resolution of the *HST* images, we identify various bright, compact sources in the central regions of HCG 16C and D, as shown in Figure 6. The exponential surface brightness profile of these sources, as well as their colors, are consistent with a star clusters, as will be discussed in Section 5.1. In order to understand the structure of these two galaxies we consider the WFPC2 imaging in the context of the double nuclei proposed for both HCG 16C and D by de Carvalho & Coziol (1999). This report was of the spectroscopic discovery of second nuclei situated 5″ west and 7″ east of the main nuclei of galaxies 16C and D, respectively. These distances are represented by the dashed blue arcs of Figure 6. The arcs are intersected by star clusters, which we mark in orange circles of diameter 3″, the width of the de Carvalho & Coziol spectroscopic aperture. At the ≈30 Mpc distance to HCG 22, the angular separations between the suggested double nuclei correspond to physical distances of 1.2 kpc and 1.7 kpc, suggestive of a major merger morphology akin to the Antennae. This is not the case in these galaxies, which instead have morphologies reminiscent of post-interaction systems, such as M82. In addition, the 1.″5 median seeing in the de Carvalho & Coziol observations would have blended the light of many sources in these crowded star-forming

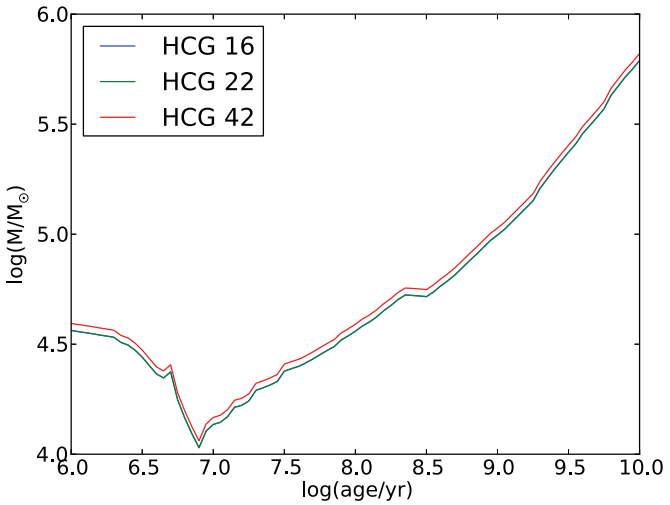

Figure 2. Conversion of $M_V = -9$ mag into mass over the full evolutionary course of a model simple stellar population (Marigo et al. 2008). As a star cluster ages it progressively loses stellar material (an effect of stellar evolution), which results in an ever decreasing mass-to-light ratio. The mass required for a star cluster to be detected therefore increases over time. In this case, we expect to detect many clusters of moderate mass in their first Gyr of evolution and only those globular clusters (age >1 Gyr) more massive than $10^5\ M_\odot$. The lines for HCGs 16 and 22 overlap.

(A color version of this figure is available in the online journal.)

inner regions, giving the semblance of a single, bright source, rather than a collection of star clusters. Our high-resolution imaging do not support the double nucleus scenario of de Carvalho & Coziol (1999) in HCG 16C and D. Finally, it is likely that the AGN-like emission-line ratios discovered by this previous work represent contamination from shocks in the galactic wind, which we know to be present from the analysis of Vogt et al. (2013).

4.2. A Tidal Feature about HCG 16A

We make use of our deep, wide-field imaging from LCO to search for low surface brightness features in the three groups. We detect a faint tail (3σ–$5\,\sigma$ level with respect to the *R*-band background) off the eastern side of 16A, shown in Figure 7. The disturbed morphology of 16B and the ring of star formation about the center of 16A suggest that the two are involved in a tidal interaction. Given that the feature is cospatial with the large H I envelope around 16A/16B (Verdes-Montenegro et al. 2001; Borthakur et al. 2010), we assume that it contains gas. Tidal features are known to be detectable for no more than ∼0.5 Gyr in the optical, after which H I is a more appropriate tracer (Mullan et al. 2011). Therefore, the proposed interaction was likely a recent one.

We perform photometry on the tail, in order to assess its age and provenance—did it originate as stripped gas in which stars subsequently formed (e.g., Hibbard et al. 1994; Knierman et al. 2003; Werk et al. 2008), or was it a stream of old stars to begin with (e.g., Gallagher & Parker 2010)? We use archival images from SDSS, as they cover a broader optical baseline than our LCO imaging and provide high-quality flat fielding. Figure 8 shows the placement of square apertures on the left (orientation has been altered for illustrative purposes) and optical colors on the right, plotted on top of a Marigo et al. (2008) SSP model track. We measure very low fluxes in these apertures (3σ–$5\,\sigma$ above background), hence the following results require confirmation from deeper imaging.[16] The measured colors are mostly representative of an aging population, between 100 Myr and 1 Gyr. We should note that it is difficult to distinguish between an aging population with a contribution from red supergiants, and a highly extinguished coeval population, based solely on *BVI* observations. Box 11, at the tip of the tail, is an exception, as its color is highly suggestive of red supergiant stars (when accounting for the reddening vector). The clumps at the extremities of tidal tails are often found to outshine their main-body counterparts and host more prolonged bursts of star formation (e.g., Mullan et al. 2011). They are also the formation sites of short-lived tidal dwarf galaxies in dynamical models (Bournaud 2010) and H I observations (e.g., Hibbard & van Gorkom 1996), although optical spectroscopy often paints a picture of tail clumps as chaotic, unbound systems (e.g., Trancho et al. 2012).

The star formation history of this debris feature, as deduced tentatively from Figure 8, characterizes it as an elusive event: an aging tidal tail with little ongoing star formation. Past optical studies of tidal debris have favored bright, blue, clumpy star-forming features as they are more readily observable. As a result, optical tails are never observed to contain stellar populations older than a few hundred Myr (Trancho et al. 2007, 2012; Bastian et al. 2009; Fedotov et al. 2011). After that stage, they are usually only observed in radio wavelengths (e.g., Hibbard et al. 2001; Koribalski & Manthey 2005), with ages between 0.5–1 Gyr (inferred mostly from dynamical modeling; e.g., Yun et al. 1994). The tail in HCG 16A is faint and smooth, and also appears to potentially be quite reddened at the $A_V \lesssim 2$ mag level—cf. $A_V < 0.5$ mag across the Mullan et al. (2011) sample. The roughly inferred age of the stellar population in the 16A tail is typical of H I tails, rather than those routinely studied in the optical. Combining all this information, we suggest that this might be a rare case of a tidal tail reaching the end of its optically detectable phase. Deeper observations are required to confirm this detection and our interpretation, while another possibility is that the feature is instead a stellar stream stripped from the early-type galaxy HCG 16B.

4.3. Other Optical Traits and Infrared Spectral Energy Distributions

All galaxies in HCG 22 display morphological peculiarities. We note a thick equatorial dust lane in galaxy 22A, observed in the past by Sparks et al. (1985), and various low surface brightness features in 22B, probably indicative of recent mergers or infall events (Figure 9). The group as a whole does not show much evidence for star formation away from the faint, extended spiral arms of 22C, which consists of a small, bright bar structure, surrounded by very faint, but orderly and symmetric, spiral arms.

HCG 42 is populated exclusively by early-type galaxies with no deviations from regular morphologies, except perhaps the seemingly "boxy" (bulge/disk) light profile of 42B. The group is dominated by 42A, which features a high luminosity and stellar mass (see Table 1).

An overall image of normality is conveyed through the IR spectral energy distributions (SEDs) of the individual galaxies in all three groups, shown in Figure 10. These follow the methodology of Gallagher et al. (2008) and combine 2MASS

[16] Toward that end, we recently obtained deep imaging as part of a Canada–France–Hawaii Telescope campaign, which will be presented in future work.

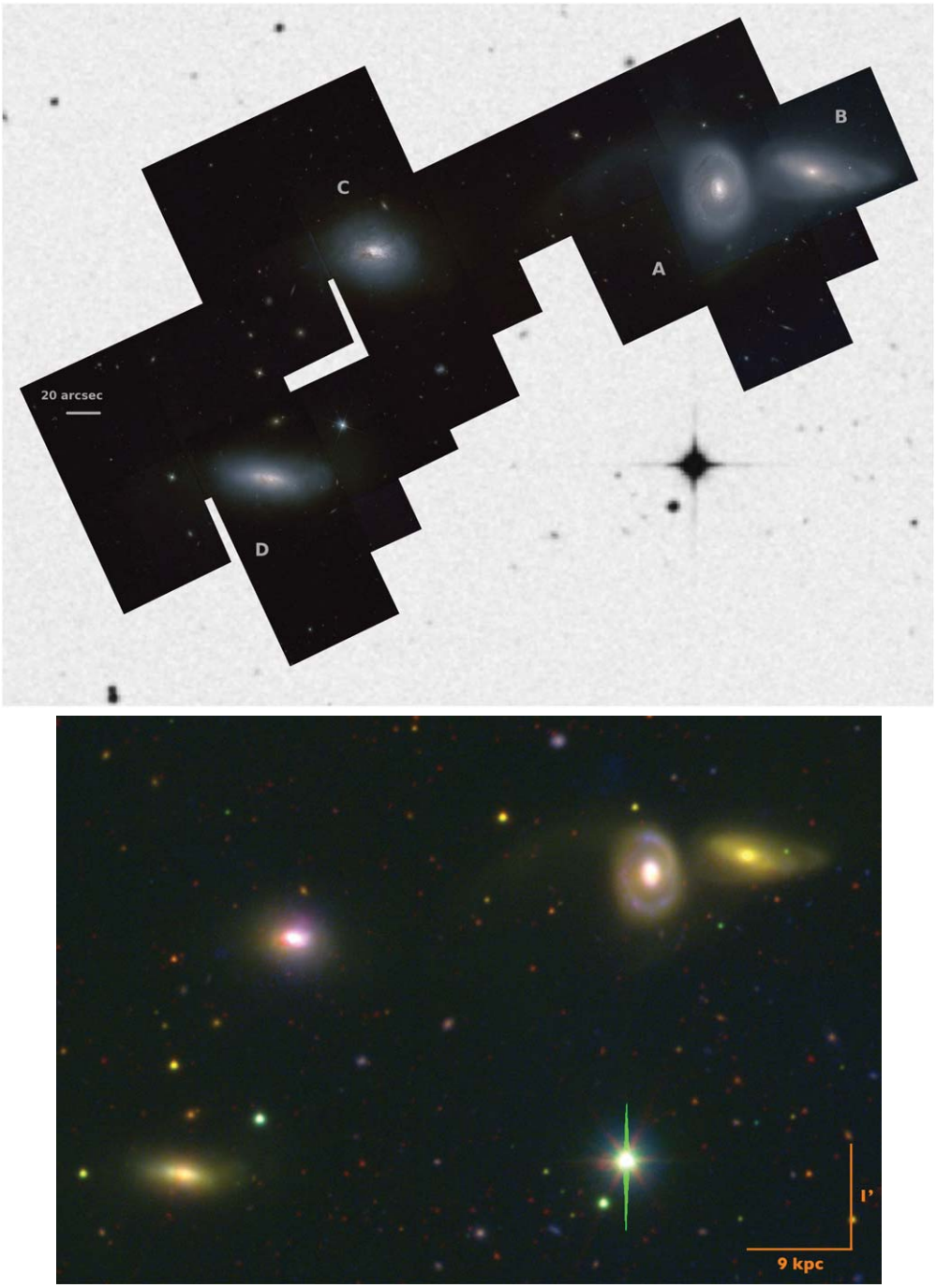

Figure 3. Top: *HST-BVI* imaging of HCG 16, framed in a DSS gray-scale background. The bottom image makes use of *Swift*-UV, LCO *R*-band, and *Spitzer* 3.6 μm frames. Star formation registers blue and cyan colors, while a yellow or red appearance reveals older stellar populations. The star-forming and interacting nature of HCG 16 is evident in this image: galaxies C and D appear patchy and dusty in the *HST* image, while galaxy B displays an asymmetric profile, despite its early-type classification. Galaxy A shows significant star formation activity in its slender spiral arms.

(A color version of this figure is available in the online journal.)

photometry in the *JHK* bands (Skrutskie et al. 2006), the four *Spitzer*-IRAC bands (3.6, 4.5, 5.8, and 8.0 μm), and 24 μm from *Spitzer*-MIPS. Each plot lists the morphological type of a galaxy next to its identifier, followed by the morphology of the plotted GRASIL model (Silva et al. 1998). We also quote $\alpha_{\rm IRAC}$ (Gallagher et al. 2008), a power-law fit to the 4.5–8.0 part of the SED, which serves as a diagnostic of star formation activity: positive values denote quiescent galaxies, while star-forming systems register negative $\alpha_{\rm IRAC}$. In previous works (especially Konstantopoulos et al. 2010), we resorted to customizing the components of each GRASIL model in order to provide an adequate description of CG galaxies. Here, the use of "standard" GRASIL templates is sufficient.

4.4. Gas Content, Cool and Hot

The H I properties of the three groups are summarized in Table 3, where we list $M_{\rm H\,I}$, the evolutionary types according to the Konstantopoulos et al. (2010) and Verdes-Montenegro et al.

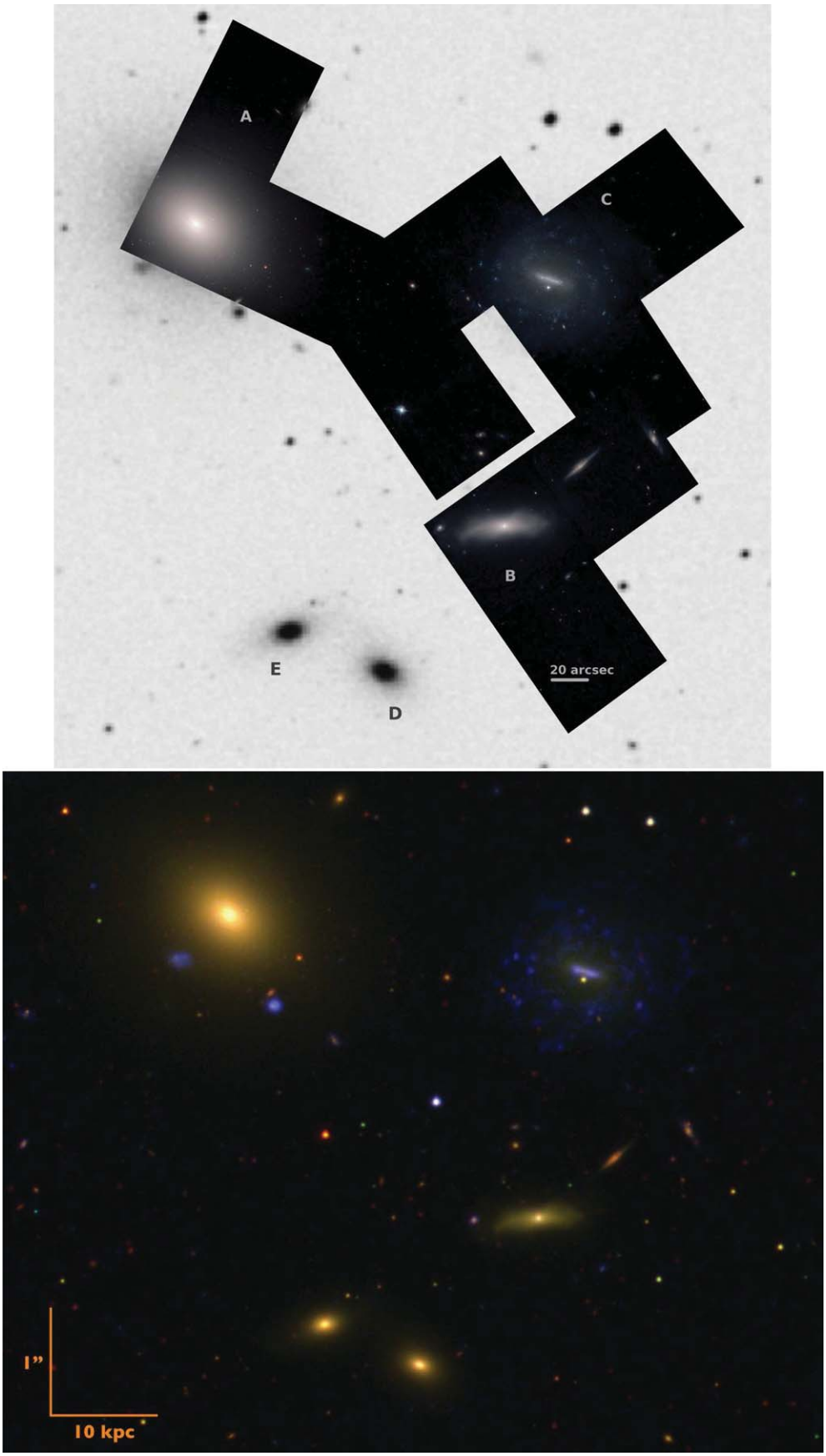

Figure 4. As in Figure 3, but for HCG 22. This group presents a more quiescent nature, with ongoing star formation only in the long network of spiral arms around galaxy C, stemming from a bright bar. Galaxies A and B appear yellow in the multi-wavelength image; however, both show indication of mergers or interactions in the past (see Figure 9): 22A displays a thick dust lane, while 22B is highly irregular. HCG 22E and D to the southeast of C are not group members but a background pair.
(A color version of this figure is available in the online journal.)

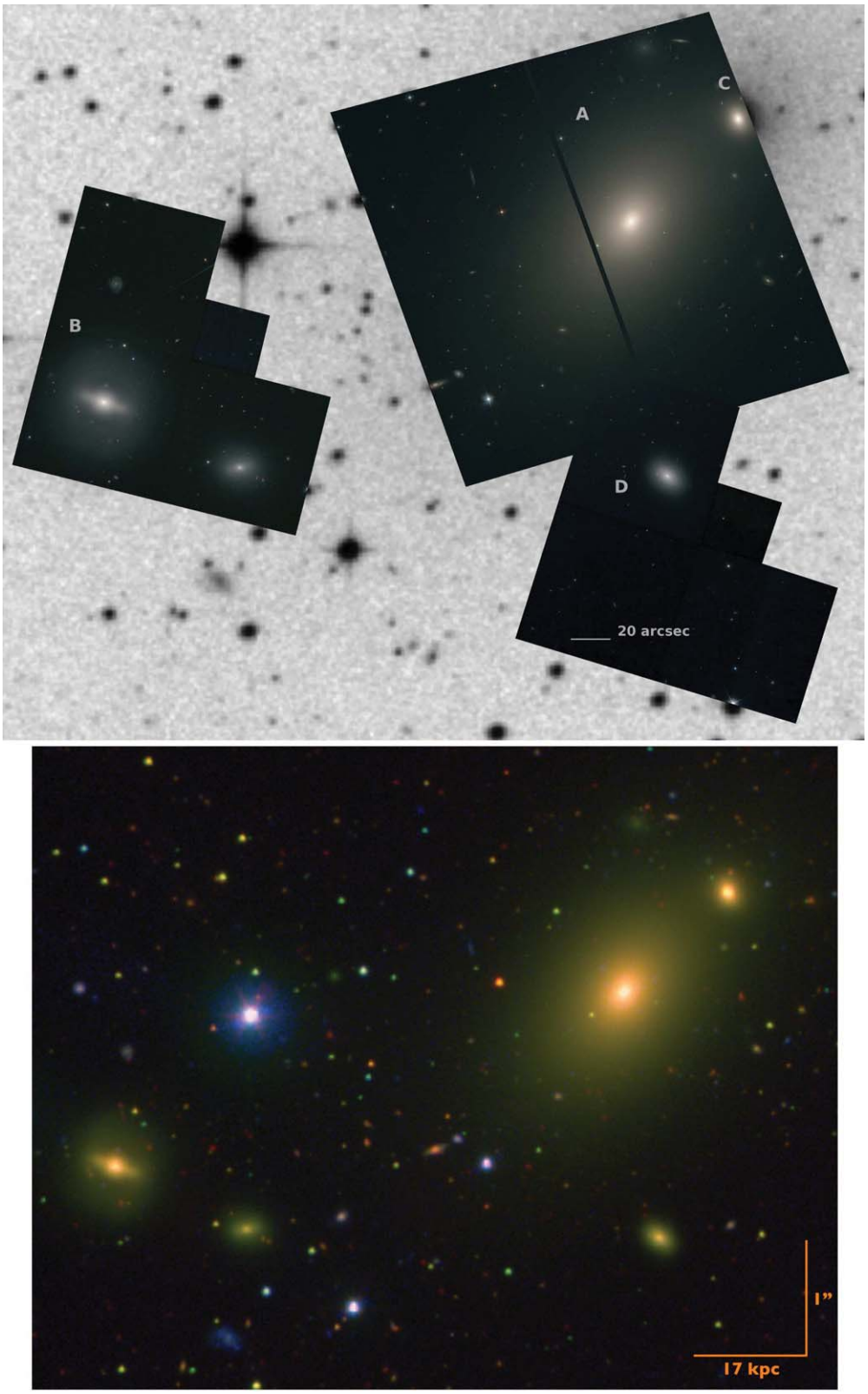

Figure 5. As in Figure 3, but for HCG 42, which is populated solely by quiescent galaxies. 42B shows a "boxy" bulge/disk morphology, while the smaller system to its west is a dwarf member (see Figure 13). We note no other peculiarities in this system.

(A color version of this figure is available in the online journal.)

(2001) classification schemes, and the $M_{\rm H\,I}$ deficiency according to Verdes-Montenegro et al. (2001; expressed as logarithmic mass in units of $M_{\odot}$). The H I morphologies are very different, from the common, extended envelope of HCG 16, to the single H I-rich galaxy of HCG 22 (22C), to the low overall content of HCG 42. The Konstantopoulos et al. (2010) scheme builds on the Johnson et al. (2007) ratios of gas-to-dynamical mass (I, II, III trace rich, intermediate, and poor groups) and further

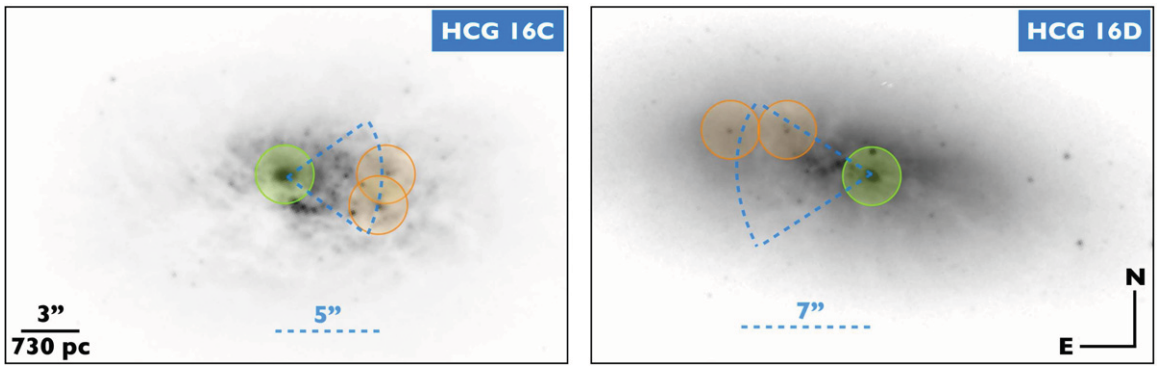

Figure 6. *HST*-WFPC2 close-up of HCG 16C and 16D in the F814W band, showing a plethora of star-forming regions. The various markings are meant to relate this imaging to the double nuclei reported by de Carvalho & Coziol (1999), with circles representing the size of the spectroscopic extraction apertures. We mark the nuclei in green circles, and then draw dashed blue arcs to indicate the suggested separation between the two nuclei (in the direction reported by de Carvalho & Coziol 1999). Orange circles mark star clusters that intersect this arc and are therefore viable candidates for the detections flagged as second nuclei. The high spatial resolution of this imaging thus argues against the interpretation of the previous work discussed. At the proposed distances from the respective nuclei of 1.2 and 1.7 kpc, the proposed second nuclei of HCG 16C and D would give rise to an Antennae-like, major merger appearance, whereas the two galaxies are more reminiscent of post-interaction systems, such as M82.

(A color version of this figure is available in the online journal.)

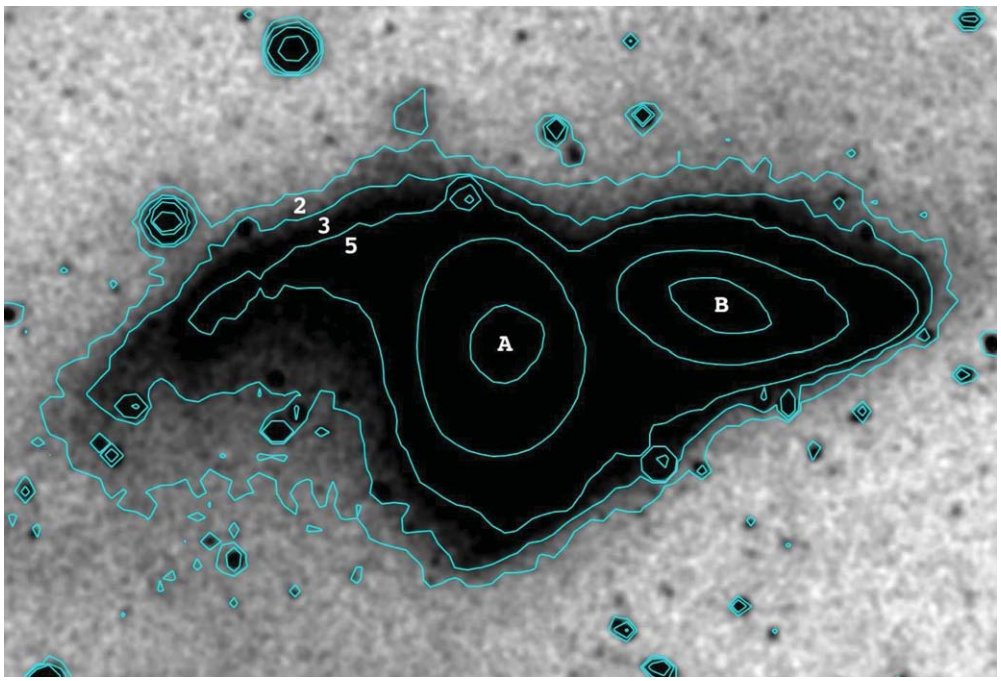

Figure 7. Smoothed, co-added LCO images in the *B* and *R* bands, presented at high contrast. North is to the top, east to the left, and the field covers a region of ≈60 × 40 kpc (or ≈250″ × 170″). The contours correspond to the *R*-band image, and numbers count the sigma level with respect to the background. A tidal feature to the east of galaxy A is detected at the 3σ–5 σ level, while the isophotes of HCG 16B are distorted.

(A color version of this figure is available in the online journal.)

divides groups according to the location of the gas: solely within galaxies (Type A) or ones with an IGM detectable in any wavelength (Type B). In summary, HCGs 16, 22, and 42 represent Types IB, IIA, and IIIA, respectively.

The properties of the hot gas in the three groups are not quite as diverse as those of the H I. The detailed analysis of Desjardins et al. (2013) detects no significant hot IGM component in the three groups, albeit the *Chandra* data of HCG 16 are perhaps too shallow to make that assessment. Diffuse X-ray emission is, however, detected around certain galaxies. The region around 42A resembles an extended envelope of hot gas, similar in appearance to those found around massive galaxies in clusters (e.g., Ponman et al. 1999). In addition, data from the Survey for Ionization in Neutral-Gas Galaxies (Meurer et al. 2006) show that the hot gas plumes observed in X-rays are coincident with Hα emission, as noted by Werk et al. (2010). Finally, Jeltema et al. (2008) presented some tentative evidence for an X-ray bridge connecting 16A and B in *Chandra* imaging.

5. STELLAR POPULATIONS

5.1. Young- and Intermediate-age Star Cluster Populations

In previous installments of this series, we have used star cluster populations to add to the characterization of CGs. They are particularly helpful in accounting for star formation in cases where our broadband metrics are contaminated by AGNs (a consideration in this case; see Table 1). Here, we take advantage of the opportunity to contrast the populations of three groups

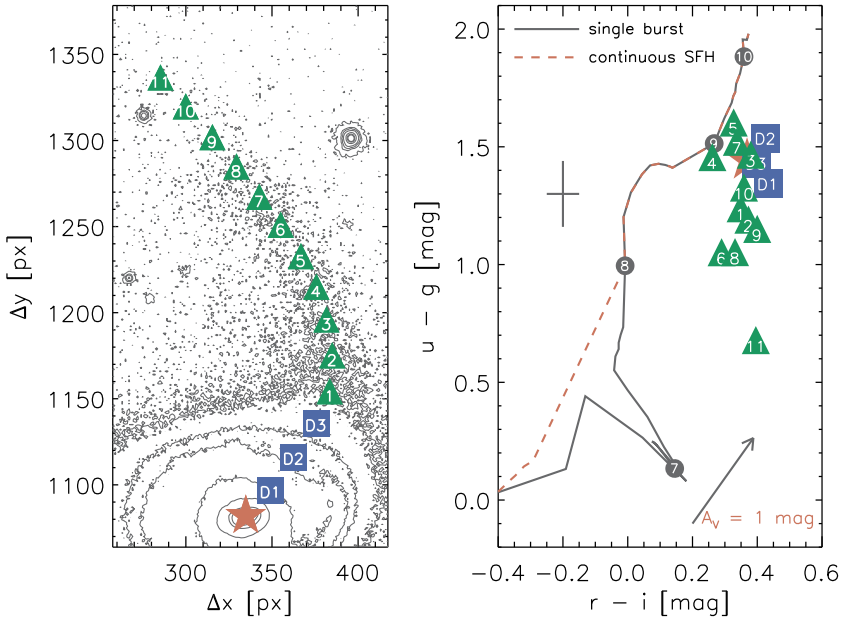

Figure 8. SDSS *ugriz* photometry of the HCG 16A tidal tail. The left panel shows a contour plot of the *r*-band SDSS image, with the location of numbered photometric apertures marked in boxes (disk), triangles (tail), and a star for the nucleus. The orientation has been adapted for illustrative purposes (east to the top, north to the right, or a clockwise 90° rotation with respect to Figure 3). Given the marginal detection, any deductions are tentative and need to be followed up with deeper imaging. The right panel shows the $u-g$ vs. $r-i$ colors of these apertures, plotted against *Yggdrasil* stellar population models representing a single burst population (solid), and a continuous star formation history (dashed). The numbers on the track denote each age dex, while the cross hair indicates typical photometric errors. When compared to simple stellar populations, most apertures appear to exhibit a relatively high dust attenuation, as demonstrated by the reddening vector, an unusual trait for tidal debris. We place the age of the underlying population between ∼100 Myr and ∼1 Gyr with no discernible age-space trends. The clump at the end of the tail is an exception, as its color suggests the presence of red supergiants and hence ongoing star formation. Deeper imaging would better constrain the age of the feature and hence the interaction that created it.

(A color version of this figure is available in the online journal.)

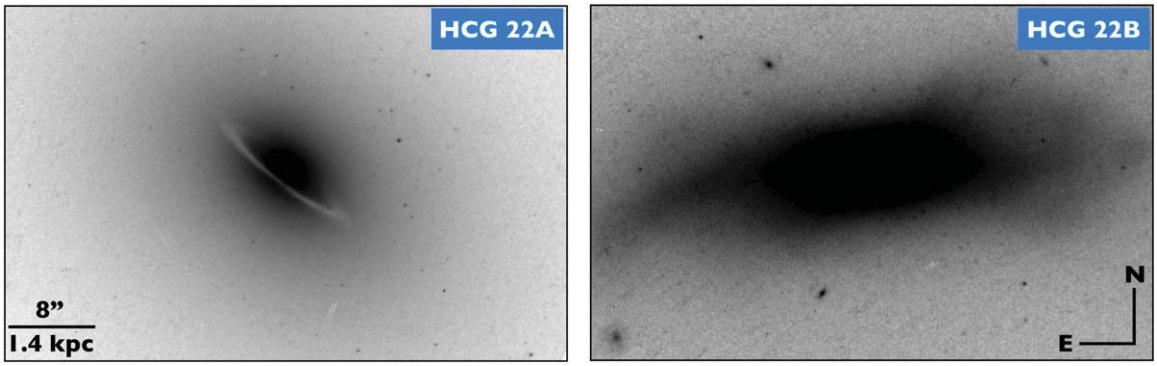

Figure 9. Left: a prominent dust lane can be seen in this *HST*-F450W image of the inner ≈2 kpc of HCG 22A, possibly the signature of a recent merger. North is to the top and east to the left of the image, as is the image on the right, where the contrast of the F814W frame has been set to demonstrate the various disturbances in the optical morphology of HCG 22B. We interpret this as the result of a recent merger (following a series of passages).

(A color version of this figure is available in the online journal.)

representing a three-stage sequence along the Konstantopoulos et al. (2010) evolutionary diagram: Types IB, IIA, and IIIA.

This sequence is largely reflected in the star cluster populations displayed in Figure 11. Here, we make use of *Yggdrasil* SSP models, as they incorporate nebular emission and continuum transmitted in the B_{450} and V_{606} filters.[17] Star clusters can be roughly age-dated through this diagram by comparing their position in color space to the SSP track, which evolves from 6 Myr to ∼10 Gyr. Specifically, HCG 16 shows evidence of star formation extending to a few Gyr into the past, with much activity over the past Gyr, consistent with star formation in the three late-type galaxies. It does not, however, show a pronounced GC clump at ages ∼10 Gyr, as one should expect from the lack of elliptical galaxies and the low overall masses of the galaxies.

In HCG 22 we detect few young clusters, with most sources found to have ages older than 1 Gyr. This denotes little activity over the past Gyr (centered around the spiral galaxy 22C, as is the H I), and pronounced star formation before that mark. It is therefore evocative of a gas-depleted system, in a fashion somewhat contrary to its Johnson et al. (2007)/Konstantopoulos et al. (2010) type. While it features two early-type galaxies among three members, it only shows a weak GC clump. While the specific frequency for GC-rich HCG 22A is consistent with its morphological type (as discussed in Section 2), the GC clump is rather weak. This is rather interesting, as galaxies are not normally found to have middle-age-heavy cluster populations

[17] In Figure 2, the nebular features were not desirable, hence we used the SSPs of Marigo et al. (2008).

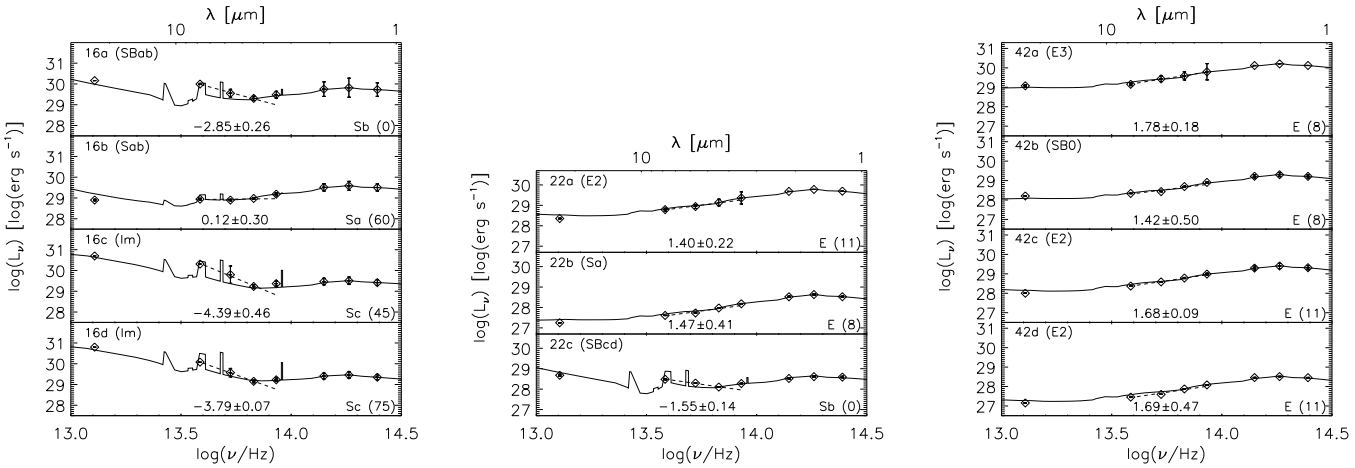

Figure 10. Infrared spectral energy distributions (SEDs) of HCGs 16, 22, and 42 (left, center, and right). The represented galaxies follow the SEDs of their nominal morphological types (marked in brackets next to the galaxy identifier), with the exception of HCG 22B, the galaxy highlighted in Figure 9 (right panel). The selected model SEDs are indicated in the bottom right of each panel, with the number in brackets indicating the logarithmic age (yr) of early-type galaxy SEDs, or the inclination of late types. The numbers below the SED mark the $\alpha_{\rm IRAC}$ diagnostic (Gallagher et al. 2008) of mid-IR activity. This is a power-law fit of the *Spitzer*-IRAC bands (4.5–8.0 μm), therefore negative values denote activity, and positive ones quiescence.

Table 3
HCGs 16, 22, and 42: H I Properties

Identifier	$\log(M_{\rm H\,I}/M_\odot)$[a]	H I Type[b]		$\delta_{\rm H\,I}$[c]	Structure
		(K10)	(VM01)	$\log(M_\odot)$	
HCG 16	14.20	IB	2	+0.41	Envelope
HCG 22	9.13	IIA	2	+0.55	Single galaxy
HCG 42	9.40	IIIA[d]	···	−0.22	Depleted

Notes.
[a] H I masses from Borthakur et al. (2010; HCG 16), Price et al. (2000; HCG 22), and Huchtmeier (1994; HCG 42).
[b] Classifications by Konstantopoulos et al. (2010) and Verdes-Montenegro et al. (2001).
[c] Deficiency in H I mass, as compared to field galaxies of matched morphological types. After Borthakur et al. (2010) and Verdes-Montenegro et al. (2001).
[d] The type of HCG 42 is uncertain, as it is not clear whether the diffuse X-ray can be attributed to the IGM or galaxy 42A alone.

(i.e., between 1 and a few Gyr old), hence HCG 22 seems to have undergone a period of intense star formation in the past (>1 Gyr). The hints of post-merger morphologies in galaxies 22A, 22B might offer a clue as to the origin of this notable star cluster population.

At the evolved end of the gas-richness sequence, HCG 42 shows little evidence of star formation in the past ∼ Gyr, with a pronounced GC clump, a distribution consistent with its IIIA evolutionary type. In this case, the areas of color space that are void are perhaps more interesting than interpreting those that are full: the absence of star clusters at ages younger than 1 Gyr indicates that star formation was essentially switched off at that point in time. This is when HCG 42 seems to have entered a different phase of evolution, one featuring little conversion of gas into stars.

In contrast with our previous studies of HCGs 7, 31, and 59 (Gallagher et al. 2010; Konstantopoulos et al. 2010, 2012), we find no large-scale star cluster complexes in these three groups (except perhaps in the spiral arms of HCG 16A). This should be expected in quiescent HCGs 22 and 42, and possibly explained by the apparently high dust content in star-forming galaxies 16C and 16D.

5.2. The Globular Cluster Population of HCG 42A

The old GCs are more difficult to study, due to the bright limiting magnitude and restricted field coverage of the WFPC2 imaging. While HCG 22A (NGC 1199) does harbor a significant GC population (Barkhouse et al. 2001), the number of GCs present in our WFPC2 data is not large enough to allow a more detailed study.

We do, however, detect a very large population of GCs in our ACS images of HCG 42A, a massive elliptical galaxy. We alter the source selection cuts of Section 3.1 to allow for the inclusion of more clusters. This is acceptable here, as GCs have very tightly confined colors. We therefore adopt a limiting magnitude of $V_{606} = 25.2$, or $M_V = 8.7$ mag at the adopted distance of 59 Mpc. We thus sample the top 15% ± 5% of the GC luminosity function, assuming a luminosity function turnover at $M_V = -7.2 \pm 0.2$ mag (e.g., Jordán et al. 2007).

We detect a total of 489 objects with GC-like colors, shown in the color–color diagram of Figure 12 (left). The $B_{435}-V_{606}$ colors from the ACS photometry were converted to Johnson–Cousins $B-I$ colors using the synthetic transformations from Sirianni et al. (2005). These colors were in turn converted to the metallicity [Fe/H] using the conversion relation from Harris et al. (2006) and gave rise to the metallicity distribution of Figure 12 (right). The histogram shows a clear bimodal distribution. An analysis according to the KMM metric of Ashman et al. (1994) reveals the peak of the "blue" GC distribution at $(B-I)_0 = 1.74$ mag, or [Fe/H] = −1.2, and that of the "red" GCs at $(B-I)_0 = 2.21$ mag, or [Fe/H] = +0.1. Related uncertainties are expected to arise from the photometric calibration and the color-to-[Fe/H] conversion, at the 0.3 dex level.

We are also able to extrapolate the total number of GCs in HCG 42A by correcting the number of detections within the ACS frame to the nominal area of the entire galaxy. We derived the radial profile of the GC system in a series of elliptical annuli with a fixed $\epsilon = 0.25$. Since our single ACS frame does not cover a background region, we used imaging of HCG 7 (from Konstantopoulos et al. 2010, at a similar distance of 65 Mpc) to estimate background contamination in each annulus, to the edge of the ACS frame (a major axis distance of 3.′7). Based on Poisson errors in the number

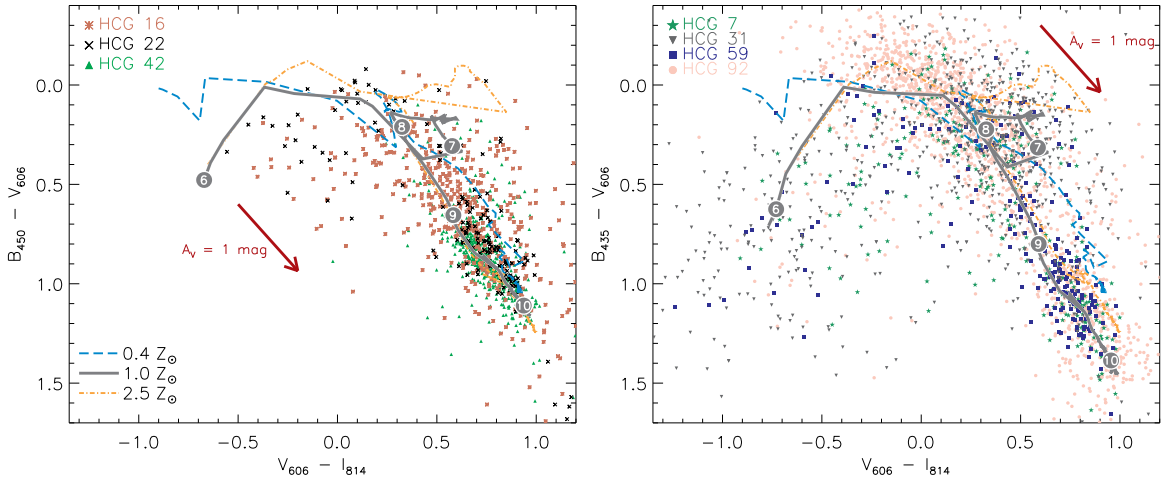

Figure 11. Star cluster candidates in HCGs 16, 22, and 42 (left, WFPC2 filters), and the combined populations of four other groups, shown on the right as a benchmark (ACS filters). The dashed, solid, and dash-dotted lines trace the evolution of *Yggdrasil* SSP models of [0.4, 1.0, 2.5] $Z_{\odot}$ (Zackrisson et al. 2011). The model tracks include nebular emission transmitted in the F435W and F606W filters at ages $\lesssim$7 Myr. The extinction vector has a length of 1 mag (A_V). Sources aligned with vectors originating on the nebular segment have ages less than $\approx$7 Myr. The relative dearth of sources in the nebular part of color space, as compared to all HCGs of the right panel, diagnoses relatively weak current star cluster formation activity throughout. The three groups display different star formation histories. HCG 16 features many clusters of supersolar metallicity, while it does not appear to host a distinct population of old globular clusters. This is to be expected, given the low galaxy masses and mainly late-type morphologies. Both HCG 22 and 42 show remarkable populations, dominated by clusters at intermediate and old ages (>1 Gyr), with only very few young clusters in HCG 22C. This is probably related to a group-wide era of merger-driven star formation in the past, consistent with the morphological types of the galaxies in these two groups, and the various signs of disturbance. From this we diagnose that HCGs 42 and two-thirds of HCG 22 entered a different mode of evolution (with little conversion of gas to stars) over the past $\sim$1 Gyr.

(A color version of this figure is available in the online journal.)

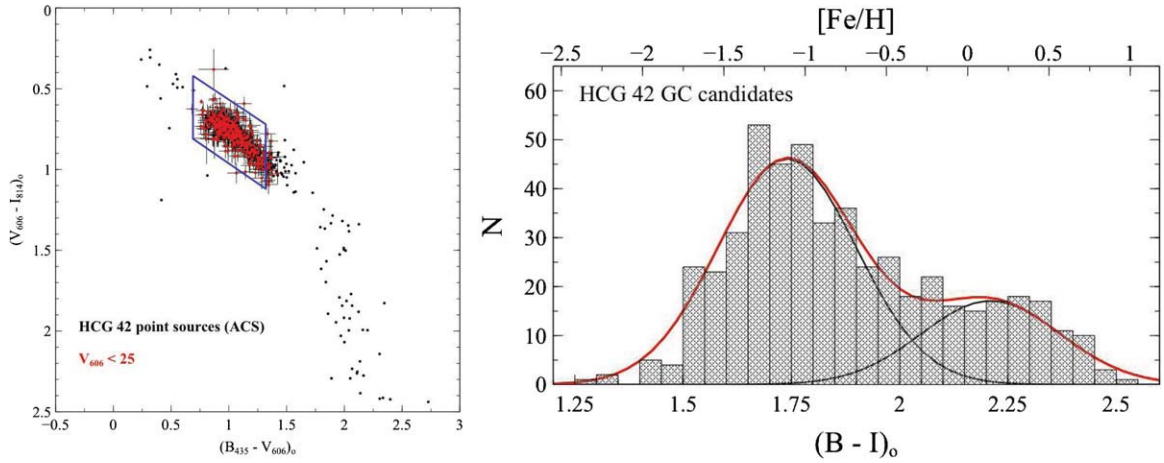

Figure 12. Globular clusters in HCG 42. Globular cluster selection (left) and color/metallicity distribution for HCG 42. The brightness cut at $m_{606} < 25$ mag corresponds to $M_{606} < -8.8$ mag, which is brighter than the peak of the GC luminosity function (e.g., Jordán et al. 2007), which complicates our interpretation. We find a bimodal distribution, common among early-type galaxies in clusters but not necessarily those in CGs (e.g., Konstantopoulos et al. 2010, 2012).

(A color version of this figure is available in the online journal.)

counts, and considering background contamination at the level of 31 ± 11 GCs, we predict a total number of clusters above the cutoff magnitude of $N_{\rm GC}^{\rm bright} = 680 \pm 63$. Adopting a completeness level of 0.9 ± 0.1 and extrapolating to the entire GC luminosity function, we derive a total GC population of HCG 42A of $N_{\rm GC} = 5030 \pm 2140$. Combined with the absolute magnitude of $M_V = -23.2$ mag[18] for the host galaxy yields a specific frequency $S_N = 2.6 \pm 1.1$ (the number of clusters per unit luminosity). All the above properties of HCG 42A, its morphology, specific frequency, GC bimodality, and location of color/metallicity peaks, are very similar to those of luminous galaxies in the cluster environment (e.g., Harris et al. 2006; Brodie & Strader 2006; Peng et al. 2006). These attributes could be related with HCG 42 being embedded in a larger structure, as will be discussed in the following section.

[18] Based on the integrated R magnitude in Table 1 and assuming $V - R = 0.5$ mag.

5.3. Dwarf Galaxies

We now turn our attention to the dwarf galaxy populations of the three HCGs. We combine information from the literature and new Hydra spectroscopy to study a total of 59 dwarf galaxies. More specifically, we incorporate the data sets of de Carvalho et al. (1997, hereafter dC97), Zabludoff & Mulchaey (2000, ZM00), and Carrasco et al. (2006), albeit for only a limited projected area about the group center. It is worth noting that the Carrasco et al. catalog builds on the previous ones and extends coverage to faint targets (down to $R \approx 21$). We also

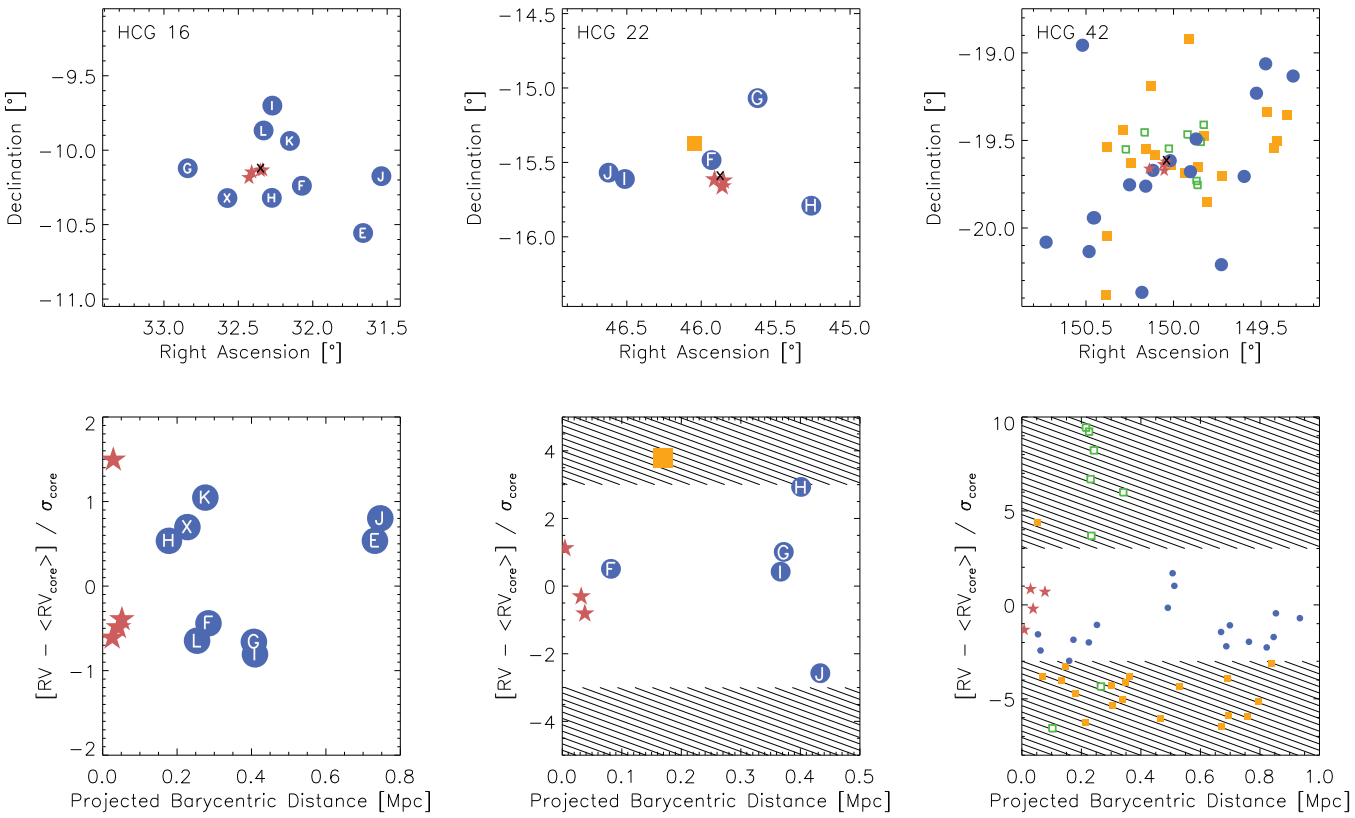

Figure 13. Diagnostic maps (top row) and phase-space diagrams (bottom row) for candidate member galaxies in HCGs 16, 22, and 42 (left, center, and right). Main members are marked with stars and their barycenter as a cross. Lettered circles and yellow boxes mark galaxies that qualify as members and associates (possible members; see Section 5.3 for details). The phase-space diagrams plot the projected distance from the group barycenter against the deviation in velocity, in terms of σ away from the main member mean. The hashed regions mark the 3σ boundary that qualifies a galaxy as a group member. HCG 16 appears to be a populous group, with seven lesser members in addition to the four main giants. Galaxy X lies at the end of the greater H I cloud that covers the main members (Verdes-Montenegro et al. 2001). HCG 22 shows five member dwarfs and one associate according to our employed diagnostic. The 3σ cut is, however, based on a small number of main galaxies, hence the associate might in reality be a member. HCG 42 is a relatively rich group, numbering 17 members and 26 associates. The open green boxes mark galaxies studied by Carrasco et al. (2006) and not included in any previous catalog. They cover a fainter part of the luminosity function than Zabludoff & Mulchaey (2000) and de Carvalho et al. (1997), albeit in a limited field of side 50′. The velocity structure appears to place the giants at the end of a large structure, perhaps a filament.

(A color version of this figure is available in the online journal.)

make use of previously unpublished velocity tables from the spectroscopic campaign that provided the basis for the Zabludoff & Mulchaey (1998, 2000) papers on poor groups (referred to as ZM98 throughout this section). Given the inhomogeneity of these collated catalogs, it is challenging to fully assess the completeness both in space and brightness. The samples are, however, complete to $R \approx 18$ mag, as they draw from the ZM00 catalogs (see their Figure 3), conditional on no galaxies having been filtered out by the ZM00 selection. Given the mean comoving radial distances to the three groups (based on redshifts from Hickson et al. 1992), this detection limit corresponds to $M_R = [-15.5, -14.7, -15.9]$ mag. The Carrasco et al. sample extends the completeness of the HCG 42 dwarf galaxy catalog to $V = 20$ mag at the 80% level ($M_V = -13.9$ mag) over a limited central area.

Figure 13 plots all galaxies within 5σ of the velocity dispersion for each group, derived from giant galaxies only. This was adapted to 10σ for HCG 42 since it is situated in a galaxy-rich region, although we note that the majority of these galaxies lie within the 5σ velocity cut. Given the large error associated with deriving a statistical dispersion from so few data points, anything in this 5σ velocity range is considered an "associate," while we enforce a 3σ criterion for membership. Associates and members are plotted as orange boxes and blue circles respectively, while the Carrasco et al. (2006) galaxies are plotted as open green boxes, to mark their different completeness level and spatial coverage. The following sections visit each group individually.

5.3.1. HCG 16

HCG 16 is covered by SDSS, so we performed a spectroscopic search in a degree-wide area centered on the group barycenter (the mass-weighted mean R.A. and decl.). We allow for a spread of $\pm 5\sigma$ about the mean redshift, representing the above-mentioned selection of group associates. The search yields four galaxies beside the four group giants, none of which were previously known to be associated with HCG 16. Furthermore, the unpublished ZM98 tables list three objects at accordant redshifts, and two galaxies from the dC97 catalog complete a set of nine dwarf members down to $M_R \approx 18$ mag. They are distributed about the giant galaxies in a roughly symmetric fashion, inside a projected area of side 0.8 Mpc. Interestingly, all these dwarfs apart from 16X lie outside the shared H I envelope of the HCG 16 giants. This might suggest that the gas originated in the individual giants and was released through interactions. The galaxies are listed in order of decreasing brightness in Table 4, derived from ZM98 photometry in the B-band (except the dC97 objects, where dC97 B-band brightness is listed). We

Table 4
Galaxies at Accordant Redshifts with HCGs 16 and 22

	ID	Coordinates		Brightness	v_R	d_{BC}	Morphology
		(h m s)	(° ′ ″)	(mag)	(km s^{-1})	(kpc)	
HCG 16							
X	NGC 848	02 10 17.6	−10 19 17.0	13.60	3989	0.23	SBab pec
E	APMUKS(BJ) B020413.18-104749.8	02 06 38.8	−10 33 23.2	15.56	3830	0.41	···
F	KUG 0205-104	02 08 17.5	−10 14 21.0	15.78	3869	0.28	···
G	KUG 0208-103	02 11 21.6	−10 07 16.3	15.89	3846	0.41	···
H	KUG 0206-105	02 09 06.0	−10 19 13.0	16.35	3971	0.18	Sc
I	KUG 0206-099A	02 09 05.2	−09 42 01.4	16.77	3830	0.41	···
J	hcg 16–10	02 08 36.8	−09 56 16.6	17.52	4000	0.18	···
K	SDSS J020836.69-095615.7	02 08 36.7	−09 56 15.8	17.63	4025	0.28	···
L	SDSS J020919.31-095202.0	02 09 19.3	−09 52 03.3	19.79	3847	0.25	S
HCG 22							
F	NGC 1209	03 06 03.1	−15 36 41.8	12.84	2690	0.38	E6?
G	NGC 1188	03 03 43.4	−15 29 04.5	14.12	2698	0.09	SAB0
H	NGC 1231	03 06 29.3	−15 34 08.4	14.32	2424	0.45	Sc
–	APMUKS(BJ) B030149.90-153401.7	03 04 10.4	−15 22 22.1	16.55	2991	0.19	···
I	APMUKS(BJ) B030008.22-151549.8	03 02 29.0	−15 04 05.8	17.19	2743	0.37	···
J	APMUKS(BJ) B025842.23-155916.7	03 01 02.4	−15 47 27.7	17.29	2913	0.38	···

Notes. Coordinates and radial velocities are drawn from previously unpublished catalogs related to Zabludoff & Mulchaey (1998), apart from: hcg 16–10 (de Carvalho et al. 1997; coordinates converted from B1950 to J2000); 16G, I, K, and L (York et al. 2000). We quote SDSS *g*-band magnitudes for HCG 16 member galaxies, with the exception of hcg 16–10, which is a *B* magnitude from de Carvalho et al. (1997). HCG 22 values are POSS photographic magnitudes (Reid & Djorgovski 1993). d_{BC} is the distance of a dwarf from the group barycenter. The morphologies of some galaxies not in the New General Catalogue were drawn from the catalogs related to Zabludoff & Mulchaey (1998). The majority were not classified, owing to the limitation of available imaging. In the case of NGC galaxies we refer to de Vaucouleurs et al. (1991).

use the Hickson (1982) naming convention to assign letters to these galaxies from E to L (assuming completeness to the faintest member). Incorporating the velocities of these nine objects increases the dynamical mass of the group by a factor of ≈4.

5.3.2. HCG 22

In HCG 22 the situation is similar, with five members and one associate, which we draw from the ZM98 tables. We employ the Hickson (1982) lettering scheme for members only. It should be noted here that the dispersion is derived from three velocities, therefore the membership of this galaxy is difficult to assess. The inclusion of just members, or all dwarfs (i.e., members and the one associate) increase the M_{dyn} by a factor of 30 or 50, respectively.

5.3.3. HCG 42

The third group, HCG 42, presents an altogether different image, with a large number of member and associate galaxies spread out widely in three dimensions. We consider 34 dwarfs from ZM00, 8 from Carrasco et al. (2006), 2 from dC97, and 1 from our Hydra redshift survey (see Table 5). These are split into 35 associates and 17 members in a relatively small projected area of 1 Mpc^2. Interestingly, the phase-space distribution of Figure 13 (right) places the four giant galaxies at the top end of the bright galaxy σ distribution—recall that the Carrasco et al. (2006) systems, marked as green boxes, are fainter than the rest. With virtually all other associates at lower redshifts, this could imply that HCG 42 is part of a larger structure that may extend to the foreground. The substructure echoes the theoretical prediction of McConnachie et al. (2009) and observational assessment of Mendel et al. (2011) who find that ∼50% of all CGs are embedded in larger structures.

In any case, HCG 42 shows not only a rich population, but also a far more complex structure than any of the five dwarf galaxy systems we have studied (those in this paper and previous works on HCGs 7 and 59; Konstantopoulos et al. 2010, 2012). The redshifts of sources plotted in Figure 13 are arranged in a continuous distribution, lending support to the interpretation that HCG 42 is a subset of a larger grouping. This might explain the extreme brightness of 42A, which is more akin to that of a bright cluster galaxy (cf. the optical brightness of M87). In addition, including all associates in an M_{dyn} calculation increases the mass by five orders of magnitude, which confirms their association not with HCG 42, but the larger collection of galaxies to which HCG 42 itself belongs. The inclusion of members only, however, leads to a physically plausible 20 fold increase. This follows on the previous finding of Rood & Struble (1994) that HCG 42 is associated with the NGC 3091 group (LGG 186 in Garcia 1993). It was noted as an "intermediate group" by de Carvalho et al. (1994).

In all, the analysis presented in this section calls for more detailed studies of the extended membership of CGs and similar aggregates. A study of morphological types is essential in this context, to relate groups to clusters and groupings of various densities. In this work, morphological typing was only possible for the few galaxies covered in our LCO imaging. Our results might also call for a refinement of the Hickson definition of CGs, given how unstable the routinely employed metrics are to the expansion of group membership.

6. SUMMARY

We have presented a multi-wavelength study of the giant and dwarf galaxies that comprise HCGs 16, 22, and 42. Our results can be summarized in three categories.

1. *Morphological characteristics and indications of past dynamical events*. Starting with an examination of large-scale morphology, we found a number of noteworthy traits among

Table 5
Galaxies at Accordant Redshifts with HCG 42

ID	Coordinates		Brightness	v_R	d_{BC}	Morphology
	(h m s)	(° ′ ″)	(mag)	(km s^{-1})	(kpc)	
[ZM00] 0003	10 00 43.3	−20 22 03.6	13.60	3977	0.70	···
[ZM00] 0005	09 59 29.0	−19 29 30.7	14.07	3853	0.69	···
[ZM00] 0015	10 01 48.3	−19 56 29.7	14.64	4081	0.49	···
[ZM00] 0017	09 58 06.3	−19 13 49.6	14.75	4049	0.85	···
[ZM00] 0022	10 00 28.2	−19 40 15.9	15.04	3879	0.76	SB0
[ZM00] 0029	10 00 38.1	−19 45 40.0	15.30	3766	0.16	dE0N
[ZM00] 0033	10 02 04.8	−18 57 22.6	15.57	4212	0.51	···
[ZM00] 0034	10 01 00.3	−19 45 12.5	15.67	3980	0.25	S0
[ZM00] 0041	09 57 16.1	−19 07 56.1	15.83	3891	0.17	···
[ZM00] 0046	09 59 36.9	−19 40 42.7	16.02	4020	0.93	dE
[ZM00] 0057	10 02 54.7	−20 04 52.1	16.22	3938	0.67	···
[ZM00] 0058	09 58 54.4	−20 12 34.0	16.28	3846	0.82	···
[ZM00] 0065	10 01 55.8	−20 08 05.0	16.43	3908	0.85	···
[ZM00] 0106	10 00 04.6	−19 36 55.4	16.88	3876	0.23	dE
[ZM00] 0143	09 58 23.1	−19 42 19.9	17.23	4287	0.51	S…/Irr
[ZM00] 0154	10 01 49.9	−19 56 32.0	17.30	3924	0.05	···
[ZM00] 0166	09 57 53.7	−19 03 45.0	17.36	3828	0.06	S
[ZM00] 0002	09 57 23.9	−19 21 16.9	12.99	3675	0.07	dE0N
[ZM00] 0006	10 01 31.2	−19 32 22.3	14.13	4587	0.05	···
[ZM00] 0009	10 00 31.5	−19 11 30.7	14.42	3675	0.36	···
[ZM00] 0013	10 01 09.1	−19 26 29.1	14.51	3442	0.69	SBd
[ZM00] 0014	09 59 13.9	−19 51 07.8	14.59	3526	0.80	S0
[ZM00] 0016	09 57 38.8	−19 30 14.1	14.67	3424	0.47	···
[ZM00] 0019	10 01 32.4	−20 23 00.0	14.82	3504	0.31	SBab
[ZM00] 0021	09 58 53.1	−19 42 19.1	14.85	3621	0.30	···
[ZM00] 0023	10 01 31.4	−20 02 34.9	15.04	3732	0.15	···
[ZM00] 0026	09 57 51.8	−19 20 18.9	15.27	3402	0.21	···
[ZM00] 0028	09 59 18.7	−19 28 22.6	15.29	3636	0.35	···
[ZM00] 0055	09 59 38.5	−18 55 14.3	16.18	3661	0.69	Sbc
[ZM00] 0059	10 00 37.7	−19 32 54.7	16.30	3434	0.76	···
[ZM00] 0069	10 00 25.0	−19 34 59.4	16.45	3647	0.13	···
[ZM00] 0085	09 59 26.5	−19 38 57.4	16.69	3538	0.34	Sb
[ZM00] 0094	09 59 44.2	−19 41 10.9	16.78	3613	0.53	···
[ZM00] 0136	10 00 03.5	−19 38 24.5	17.14	3748	0.84	Sc
Hydra 0030	10 00 58.0	−19 37 44.3	19.14	3571	0.18	···
[C06] 2190	09 59 28.5	−19 43 53.0	18.56	4768	0.34	···
[C06] 1089	09 59 27.1	−19 45 16.0	18.69	3614	0.27	···
[C06] 0694	10 00 06.4	−19 32 49.0	18.69	5017	0.24	···
[C06] 2123	10 00 39.6	−19 27 15.0	19.75	5128	0.23	···
[C06] 1345	09 59 18.6	−19 24 38.0	19.81	4509	0.23	···
[C06] 2234	09 59 22.7	−19 30 29.0	20.25	3366	0.10	···
[C06] 0760	10 01 05.4	−19 33 04.0	20.27	5152	0.22	···
[C06] 1869	09 59 40.8	−19 27 57.0	20.70	4846	0.23	···

Notes. Top tier: members, bottom: associates. ZM00 and C06 list the *R* and *V* bands, respectively. Hydra 0030 photometry is in the *R* band. Morphologies from de Vaucouleurs et al. (1991), apart from [ZM00] 0046 and [ZM00] 0106, characterized using our LCO images.

11 giant galaxies. HCG 16B is lopsided, perhaps as a result of a recent interaction with 16A. Galaxies 16C and 16D present irregular morphologies from the ultraviolet to the infrared. HCG 16D is known to exhibit X-ray emission consistent with the Hα emission detected by Werk et al. (2010) in the form of a supergalactic wind (Rich et al. 2010; Vogt et al. 2013). The "secondary nuclei" reported by de Carvalho & Coziol (1999) are likely to be agglomerates of star clusters whose light was blended by the 1.″5 seeing.

Within the large H I envelope of HCG 16 we also find a tidal tail, extending to the east of 16A. While our interpretation needs to be confirmed with deeper imaging, this feature presents a good opportunity to study a debris feature at the end of its optically detectable phase. We find a hint of ongoing star formation at the tip of the tail, while the rest of the feature appears to host a $\lesssim$1 Gyr old stellar population. The existing data do not allow us to discern between different evolutionary scenarios—old stars stripped in an interaction versus in-situ star formation a long time ago.

All three galaxies in HCG 22 display interesting traits: the equatorial dust ring in 22A and the network of low surface brightness features around 22B are consistent with recent merger or infall events, while the bright central bar and extremely faint, loose network of spiral arms of 22C represent the only sites of star formation in the system—and

also where all the H I is situated. The galaxies of HCG 42 do not display any diversions from quiescence.

2. *Star cluster populations and star formation histories*. The evolutionary sequence mapped out by the three CGs in terms of gas richness is reflected in the star clusters. The color distribution of the cluster populations portray a "young" HCG 16 that has yet to develop a large GC population, as opposed to "old" HCG 42, where the bimodal GC population accounts for the majority of detected sources. There is a distinct lack of young clusters here (<1 Gyr), which temporally marks the quenching of star formation in HCG 42. In between the two groups is HCG 22, which hosts a very unusual stellar population, dominated by clusters of intermediate age. This reveals that the bulk of star formation activity happened over the past few Gyr, with little recent activity, practically none outside the spiral arms of 22C. To our knowledge, no individual galaxy or grouping has been found to host such a markedly intermediate-age population. This is an observer bias introduced by the preferential study of the young cluster populations of either mergers and highly star-forming systems, or the GC populations of early-type galaxies. From their morphologies, we propose that galaxies 22A and 22B are recent merger remnants. The star cluster populations are consistent with this scenario.

   The above provides a good demonstration of the utility of star clusters as chronometers for past star formation events. Any epoch at which a galaxy exhibits a significant SFR will be recorded by the star clusters, and bursts will register as "bumps" along the model track (see the analysis of Stephan's Quintet by Fedotov et al. 2011). Equally important is the dearth or absence of clusters in certain parts of color space, indicating a low or zero SFR, such as HCG 42. This provides an estimate of the time when a system entered a mode of galaxy evolution where no more gas is being converted to stars. At this stage, any gas in the IGM can only be redistributed or heated.

3. *Dwarf galaxy membership and implications*. The information on dwarf galaxies collected in this study originates from a variety of sources, however, all utilized catalogs are complete to $R \simeq 18$ mag, or $M_R = [-15.5, -14.7, -15.9]$ mag. This gives us the opportunity to study the bright end of the dwarf galaxy luminosity function and place the three groups in the context of the distinction between isolated and embedded groups (McConnachie et al. 2009; Mendel et al. 2011). HCGs 16 displays a more or less symmetric spatial distribution of dwarfs, albeit all but one (HCG 16X) lie outside the H I envelope shared by the giants. This might indicate that the gas was released through interactions between the giants. The phase-space diagram of HCG 42 places it at the end of a filament or other complex velocity structure made of ≈50 dwarf galaxies.

   We made two cuts in velocity space, at 3σ and 10σ, to sort between members and "associates." This way we were able to test the applicability of the velocity dispersion, designed to characterize populous galaxy clusters, in studying small groups. In other words, what is the meaning of a velocity dispersion derived from only four galaxies? This question is especially relevant seeing as CGs are not necessarily expected to be dynamically relaxed.

   Indeed, the inclusion of all "associate" dwarf galaxy velocities gives rise to a tremendous change in the inferred dynamical properties of the three groups. The dynamical masses ($M_{\rm dyn}$, which are only truly appropriate for virialized systems) increase by factors of 4, 50, and a gargantuan 10^5 for HCGS 16, 22, and 42. In contrast, including only high-confidence members (the 3σ cut) only increases the $M_{\rm dyn}$ by a factor of ∼10 for all three groups. This indicates that, although flawed from a statistical perspective, the velocity dispersion of the group core might provide a reliable metric. More groups need to be studied in order to ascertain this eventuality.

   Another way to examine this effect of dwarfs on the $M_{\rm dyn}$ derivation is in terms of the hierarchy in which a group is found. While the isolated HCGs 16 and 22 are mildly affected by the inclusion of dwarfs *and* associates, the derivation of $M_{\rm dyn}$ breaks down for embedded HCG 42. In all, we find that updating the velocity dispersion through the careful inclusion of high-confidence dwarf members vastly upgrades its value by making it a statistically viable metric.

We thank the anonymous referee for the enthusiastic reception of our work and for suggestions that improved the manuscript. Funding was provided at PSU by the National Science Foundation under award AST-0908984. Support for this work was provided by NASA through grant No. HST-GO-10787.15-A from the Space Telescope Science Institute which is operated by AURA, Inc., under NASA contract NAS 5-26555. K.F. and S.C.G. thank the Natural Science and Engineering Research Council of Canada and the Ontario Early Researcher Award Program for support. This paper makes use of publicly available SDSS imaging and spectroscopy. Funding for the creation and distribution of the SDSS Archive has been provided by the Alfred P. Sloan Foundation, the Participating Institutions, the National Aeronautics and Space Administration, the National Science Foundation, the U.S. Department of Energy, the Japanese Monbukagakusho, and the Max Planck Society. The SDSS Web site is http://www.sdss.org/. The SDSS is managed by the Astrophysical Research Consortium (ARC) for the Participating Institutions. The Participating Institutions are The University of Chicago, Fermilab, the Institute for Advanced Study, the Japan Participation Group, The Johns Hopkins University, Los Alamos National Laboratory, the Max-Planck-Institute for Astronomy (MPIA), the Max-Planck-Institute for Astrophysics (MPA), New Mexico State University, Princeton University, the United States Naval Observatory, and the University of Washington. This research has made use of the NASA/IPAC Extragalactic Database (NED) which is operated by the Jet Propulsion Laboratory, California Institute of Technology, under contract with the National Aeronautics and Space Administration.

REFERENCES

Ashman, K. M., Bird, C. M., & Zepf, S. E. 1994, AJ, 108, 2348
Bahcall, N. A., Harris, D. E., & Rood, H. J. 1984, ApJL, 284, L29
Barkhouse, W. A., West, M. J., & Bothun, G. D. 2001, ApJ, 562, 679
Barton, E., Geller, M., Ramella, M., Marzke, R. O., & da Costa, L. N. 1996, AJ, 112, 871
Bastian, N., Trancho, G., Konstantopoulos, I. S., & Miller, B. W. 2009, ApJ, 701, 607
Belsole, E., Sauvageot, J.-L., Ponman, T. J., & Bourdin, H. 2003, A&A, 398, 1
Bitsakis, T., Charmandaris, V., da Cunha, E., et al. 2011, A&A, 533, A142
Borthakur, S., Yun, M. S., & Verdes-Montenegro, L. 2010, ApJ, 710, 385
Bournaud, F. 2010, in Proc. ASP Conf. Ser. Vol. 423, Galaxy Wars: Stellar Populations and Star Formation in Interacting Galaxies, ed. B. Smith, N. Bastian, S. J. U. Higdon, & J. L. Higdon (San Francisco, CA: ASP), 177
Brodie, J. P., & Strader, J. 2006, ARA&A, 44, 193
Carrasco, E. R., Mendes de Oliveira, C., & Infante, L. 2006, AJ, 132, 1796
Cluver, M. E., Appleton, P. N., Ogle, P., et al. 2013, ApJ, 765, 93

Da Rocha, C., & Mendes de Oliveira, C. 2005, MNRAS, 364, 1069
Da Rocha, C., Mendes de Oliveira, C., Bolte, M., Ziegler, B. L., & Puzia, T. H. 2002, AJ, 123, 690
Da Rocha, C., Mieske, S., Georgiev, I. Y., et al. 2011, A&A, 525, A86
de Carvalho, R. R., & Coziol, R. 1999, AJ, 117, 1657
de Carvalho, R. R., Ribeiro, A. L. B., Capelato, H. V., & Zepf, S. E. 1997, ApJS, 110, 1
de Carvalho, R. R., Ribeiro, A. L. B., & Zepf, S. E. 1994, ApJS, 93, 47
de Vaucouleurs, G., de Vaucouleurs, A., Corwin, H. G., Jr., et al. 1991, Third Reference Catalogue of Bright Galaxies (New York: Springer)
Desjardins, T. D., Gallagher, S. C., Tzanavaris, P., et al. 2013, ApJ, 763, 121
Dolphin, A. E. 2000, PASP, 112, 1397
Doyle, M. T., Drinkwater, M. J., Rohde, D. J., et al. 2005, MNRAS, 361, 34
Emsellem, E., Cappellari, M., Krajnović, D., et al. 2011, MNRAS, 414, 888
Evans, I. N., Primini, F. A., Glotfelty, K. J., et al. 2010, ApJS, 189, 37
Fedotov, K., Gallagher, S. C., Konstantopoulos, I. S., et al. 2011, AJ, 142, 42
Gallagher, J. S., III, & Parker, A. 2010, ApJ, 722, 1962
Gallagher, S. C., Durrell, P. R., Elmegreen, D. M., et al. 2010, AJ, 139, 545
Gallagher, S. C., Johnson, K. E., Hornschemeier, A. E., Charlton, J. C., & Hibbard, J. E. 2008, ApJ, 673, 730
Garcia, A. M. 1993, A&AS, 100, 47
Harris, W. E., Whitmore, B. C., Karakla, D., et al. 2006, ApJ, 636, 90
Hibbard, J. E., Guhathakurta, P., van Gorkom, J. H., & Schweizer, F. 1994, AJ, 107, 67
Hibbard, J. E., & van Gorkom, J. H. 1996, AJ, 111, 655
Hibbard, J. E., van Gorkom, J. H., Rupen, M. P., & Schiminovich, D. 2001, in ASP Conf. Ser. 240, Gas and Galaxy Evolution, ed. J. E. Hibbard, M. Rupen, & J. H. van Gorkom (San Francisco, CA: ASP), 657
Hickson, P. 1982, ApJ, 255, 382
Hickson, P., Kindl, E., & Auman, J. R. 1989, ApJS, 70, 687
Hickson, P., Mendes de Oliveira, C., Huchra, J. P., & Palumbo, G. G. 1992, ApJ, 399, 353
Huchtmeier, W. K. 1994, A&A, 286, 389
Hunsberger, S. D., Charlton, J. C., & Zaritsky, D. 1998, ApJ, 505, 536
Jeltema, T. E., Binder, B., & Mulchaey, J. S. 2008, ApJ, 679, 1162
Johnson, K. E., Hibbard, J. E., Gallagher, S. C., et al. 2007, AJ, 134, 1522
Jordán, A., McLaughlin, D. E., Côté, P., et al. 2007, ApJS, 171, 101
Knierman, K. A., Gallagher, S. C., Charlton, J. C., et al. 2003, AJ, 126, 1227
Konstantopoulos, I. S., Bastian, N., Smith, L. J., et al. 2009, ApJ, 701, 1015
Konstantopoulos, I. S., Fedotov, K., Gallagher, S. C., et al. 2011, in Stellar Clusters & Associations: A RIA Workshop on Gaia, ed. E. J. Navarro, A. T. Gallego Calvente, & M. R. Zapatero Osorio, 133
Konstantopoulos, I. S., Gallagher, S. C., Fedotov, K., et al. 2010, ApJ, 723, 197
Konstantopoulos, I. S., Gallagher, S. C., Fedotov, K., et al. 2012, ApJ, 745, 30
Konstantopoulos, I. S., Smith, L. J., Adamo, A., et al. 2013, AJ, 145, 137
Koribalski, B., & Manthey, E. 2005, MNRAS, 358, 202
Larsen, S. S. 1999, A&AS, 139, 393
Marigo, P., Girardi, L., Bressan, A., et al. 2008, A&A, 482, 883
McConnachie, A. W., Ellison, S. L., & Patton, D. R. 2008, MNRAS, 387, 1281
McConnachie, A. W., Patton, D. R., Ellison, S. L., & Simard, L. 2009, MNRAS, 395, 255
Mendel, J. T., Ellison, S. L., Simard, L., Patton, D. R., & McConnachie, A. W. 2011, MNRAS, 418, 1409
Meurer, G. R., Hanish, D. J., Ferguson, H. C., et al. 2006, ApJS, 165, 307
Mobasher, B., Colless, M., Carter, D., et al. 2003, ApJ, 587, 605
Monnier Ragaigne, D., van Driel, W., Schneider, S. E., Balkowski, C., & Jarrett, T. H. 2003, A&A, 408, 465
Mullan, B., Konstantopoulos, I. S., Kepley, A. A., et al. 2011, ApJ, 731, 93
Palma, C., Zonak, S. G., Hunsberger, S. D., et al. 2002, AJ, 124, 2425
Paturel, G., Theureau, G., Bottinelli, L., et al. 2003, A&A, 412, 57
Peng, E. W., Jordán, A., Côté, P., et al. 2006, ApJ, 639, 95
Ponman, T. J., Cannon, D. B., & Navarro, J. F. 1999, Natur, 397, 135
Poole, T. S., Breeveld, A. A., Page, M. J., et al. 2008, MNRAS, 383, 627
Price, R. M., Babic, B., & Jones, K. 2000, in ASP Conf. Ser. 209, IAU Colloq. 174: Small Galaxy Groups, ed. M. J. Valtonen & C. Flynn (San Francisco, CA: ASP), 163
Reid, N., & Djorgovski, S. 1993, in ASP Conf. Ser. 43, Sky Surveys. Protostars to Protogalaxies, ed. B. T. Soifer (San Francisco, CA: ASP), 125
Ribeiro, A. L. B., de Carvalho, R. R., Coziol, R., Capelato, H. V., & Zepf, S. E. 1996, ApJL, 463, L5
Rich, J. A., Dopita, M. A., Kewley, L. J., & Rupke, D. S. N. 2010, ApJ, 721, 505
Rood, H. J., & Struble, M. F. 1994, PASP, 106, 413
Schweizer, F. 2004, in ASP Conf. Ser. 322, The Formation and Evolution of Massive Young Star Clusters, ed. H. J. G. L. M. Lamers, L. J. Smith, & A. Nota (San Francisco, CA: ASP), 111
Silva, L., Granato, G. L., Bressan, A., & Danese, L. 1998, ApJ, 509, 103
Sirianni, M., Jee, M. J., Benítez, N., et al. 2005, PASP, 117, 1049
Skrutskie, M. F., Cutri, R. M., Stiening, R., et al. 2006, AJ, 131, 1163
Sparks, W. B., Wall, J. V., Thorne, D. J., et al. 1985, MNRAS, 217, 87
Sulentic, J. W., Pietsch, W., & Arp, H. 1995, A&A, 298, 420
Torres-Flores, S., Mendes de Oliveira, C., de Mello, D. F., et al. 2009, A&A, 507, 723
Trancho, G., Bastian, N., Schweizer, F., & Miller, B. W. 2007, ApJ, 658, 993
Trancho, G., Konstantopoulos, I. S., Bastian, N., et al. 2012, ApJ, 748, 102
Turner, M. J. L., Reeves, J. N., Ponman, T. J., et al. 2001, A&A, 365, L110
Tzanavaris, P., Hornschemeier, A. E., Gallagher, S. C., et al. 2010, ApJ, 716, 556
Verdes-Montenegro, L., Yun, M. S., Williams, B. A., et al. 2001, A&A, 377, 812
Vogt, F. P. A., Dopita, M. A., & Kewley, L. J. 2013, ApJ, 768, 151
Walker, L. M., Johnson, K. E., Gallagher, S. C., et al. 2010, AJ, 140, 1254
Walker, L. M., Johnson, K. E., Gallagher, S. C., et al. 2012, AJ, 143, 69
Werk, J. K., Putman, M. E., Meurer, G. R., et al. 2008, ApJ, 678, 888
Werk, J. K., Putman, M. E., Meurer, G. R., et al. 2010, AJ, 139, 279
White, P. M., Bothun, G., Guerrero, M. A., West, M. J., & Barkhouse, W. A. 2003, ApJ, 585, 739
York, D. G., Adelman, J., Anderson, J. E., Jr., et al. 2000, AJ, 120, 1579
Yun, M. S., Ho, P. T. P., & Lo, K. Y. 1994, Natur, 372, 530
Zabludoff, A. I., & Mulchaey, J. S. 1998, ApJ, 496, 39
Zabludoff, A. I., & Mulchaey, J. S. 2000, ApJ, 539, 136
Zackrisson, E., Rydberg, C.-E., Schaerer, D., Östlin, G., & Tuli, M. 2011, ApJ, 740, 13